

AD _____

Award Number: W81XWH-13-1-0105

TITLE: Targeting Metabolic Survival Pathways in Lung Cancer via Combination Therapy

PRINCIPAL INVESTIGATOR: Christian Metallo

CONTRACTING ORGANIZATION: University of California, San Diego
La Jolla, CA 92093

REPORT DATE: June-2014

TYPE OF REPORT: Annual

PREPARED FOR: U.S. Army Medical Research and Materiel Command
Fort Detrick, Maryland 21702-5012

DISTRIBUTION STATEMENT: Approved for Public Release;
Distribution Unlimited

The views, opinions and/or findings contained in this report are those of the author(s) and should not be construed as an official Department of the Army position, policy or decision unless so designated by other documentation.

REPORT DOCUMENTATION PAGE			<i>Form Approved</i> <i>OMB No. 0704-0188</i>		
Public reporting burden for this collection of information is estimated to average 1 hour per response, including the time for reviewing instructions, searching existing data sources, gathering and maintaining the data needed, and completing and reviewing this collection of information. Send comments regarding this burden estimate or any other aspect of this collection of information, including suggestions for reducing this burden to Department of Defense, Washington Headquarters Services, Directorate for Information Operations and Reports (0704-0188), 1215 Jefferson Davis Highway, Suite 1204, Arlington, VA 22202-4302. Respondents should be aware that notwithstanding any other provision of law, no person shall be subject to any penalty for failing to comply with a collection of information if it does not display a currently valid OMB control number. PLEASE DO NOT RETURN YOUR FORM TO THE ABOVE ADDRESS.					
1. REPORT DATE June 2014		2. REPORT TYPE Annual		3. DATES COVERED 01-June-2013 to 31-May-2014	
4. TITLE AND SUBTITLE Targeting Metabolic Survival Pathways in Lung Cancer via Combination Therapy			5a. CONTRACT NUMBER W81XWH-13-1-0105		
			5b. GRANT NUMBER W81XWH-13-1-0105		
			5c. PROGRAM ELEMENT NUMBER		
6. AUTHOR(S) Christian M. Metallo, Hui Zhang, Seth Parker, Christopher Ahn, Reuben Shaw E-Mail: cmetallo@ucsd.edu			5d. PROJECT NUMBER		
			5e. TASK NUMBER		
			5f. WORK UNIT NUMBER		
7. PERFORMING ORGANIZATION NAME(S) AND ADDRESS(ES) University of California, San Diego 9500 Gilman Drive, MC-0412 La Jolla, CA 92093			8. PERFORMING ORGANIZATION REPORT NUMBER		
9. SPONSORING / MONITORING AGENCY NAME(S) AND ADDRESS(ES) U.S. Army Medical Research and Materiel Command Fort Detrick, Maryland 21702-5012			10. SPONSOR/MONITOR'S ACRONYM(S)		
			11. SPONSOR/MONITOR'S REPORT NUMBER(S)		
12. DISTRIBUTION / AVAILABILITY STATEMENT Approved for Public Release; Distribution Unlimited					
13. SUPPLEMENTARY NOTES					
14. ABSTRACT This proposal aims to identify critical metabolic pathways necessary for survival of liver kinase B1 (LKB1)-deficient non-small cell lung cancer (NSCLC) cell lines. We have conducted 13C metabolic flux analysis studies in LKB1 proficient or deficient NSCLC cells under nutrient complete or metabolic stress conditions (e.g. hypoxia, matrix detachment). Using these analyses we can demonstrate that cells lacking the LKB1 tumor suppressor exhibit limited oxidation of glucose-derived pyruvate in mitochondria. LKB1-deficient cells also exhibit increased reliance on glutamine metabolism. Treatment with biguanides such as metformin or phenformin decreases oxidative mitochondrial metabolism. A critical defect we have observed in our analyses is the inability of LKB1-deficient tumor cells to recover in response to phenformin treatment, as carbohydrate oxidation remains compromised for an extended period of time after removal/washout of phenformin. Given the dependence of LKB1-deficient tumor cells on glutamine metabolism, we are targeting a critical enzyme responsible for catalyzing the entry of glutamine carbon into the Krebs cycle in mitochondria, glutaminase.					
15. SUBJECT TERMS Metabolic stress, liver kinase B1, non-small cell lung cancer, glutamine metabolism, biguanides					
16. SECURITY CLASSIFICATION OF:			17. LIMITATION OF ABSTRACT	18. NUMBER OF PAGES	19a. NAME OF RESPONSIBLE PERSON
a. REPORT	b. ABSTRACT	c. THIS PAGE			USAMRMC
U	U	U	UU	37	19b. TELEPHONE NUMBER (include area code)

Table of Contents

	<u>Page</u>
Introduction.....	4
Body.....	4
Key Research Accomplishments.....	10
Reportable Outcomes.....	10
Conclusion.....	10
References.....	11
Appendices.....	12

Introduction

The metabolic requirements of cancer cells are different than those of normal tissues [1, 2]. For example, the liver kinase B1 (LKB1) tumor suppressor protein is dysfunctional in approximately 30% of non-small cell lung carcinomas (NSCLCs) and plays a critical role in the cellular response to energy stress [3]. Defects in such metabolic regulation may serve as potential points for therapeutic intervention. To exploit this phenomenon we must identify the most highly activated metabolic fluxes in cancer cells as a function of their genetic background (e.g. functional status of the LKB1-deficient tumor suppressor) and stress level. Systems-based approaches are required to quantitatively describe these interconnected pathways in sufficient detail to determine optimal enzyme targets under conditions of stress [4]. We hypothesize that combining these compounds with inhibitors of glutamine metabolism will be an effective therapy for LKB1-deficient lung tumors. The objective of this research is to identify metabolic susceptibilities in LKB1-deficient NSCLC using systems-level metabolic flux analysis. Subsequent studies in Year 2 of this grant will aim to design combinatorial treatments that simultaneously induce these dependencies and target compensatory pathways.

Body

A description of specific results associated with each Task scheduled for Year 1 is included below. Tasks with work completed or in progress are in black and those tasks scheduled for completion in Year 2 are in gray font.

- Task 1. Perform systems-level metabolic analysis of isogenic NSCLC cell lines expressing or lacking functional LKB1 using isotope tracers. Lines to be studied include vector control (LKB1-deficient), wild-type (WT) LKB1, and kinase dead (KD) LKB1-expressing A549 cells. Work to be performed by Hui Zhang and graduate student to be named (Seth Parker) (months 1-6)
- 1a. Generate ^{13}C -labeling data in the above cell lines using glucose and glutamine tracers under conditions of nutrient withdrawal and hypoxia (months 1-4).
 - 1b. Measure nutrient uptake and byproduct secretion rates under the above conditions (months 1-4).
 - 1c. Validate signaling downstream of LKB under the above conditions (months 1-4).
 - 1d. Perform computational analyses of these data to generate comprehensive flux maps of NSCLC cells +/- LKB1 (months 3-6).

We have completed extensive studies comparing A549 cells engineered with an empty pBABE control vector (vec.) versus those expressing function (wild-type) LKB1 protein (+LKB1). These results are presented in Figure 1 below. Although the cells grow identically in culture (Figure 1A), addition of functional LKB1 to deficient cells changes intracellular metabolic pathway activity. Signaling analysis via Western blot indicated that +LKB1 cells expressed high levels of the tumor suppressor protein (Figure 1B). Culture of cells in the presence of $[^{13}\text{C}]$ glucose (blue circles) or $[^{13}\text{C}]$ glutamine (green circles) and mass spectrometry analysis (Figure 1C, circles represent labeled/filled or unlabeled/open). Quantitation of labeling in TCA intermediates provides a relative indication of metabolic flux from tracers to specific metabolites. For example, citric acid labeling from $[^{13}\text{C}]$ glucose is significantly increased in +LKB1 cells, suggesting that flux through the pyruvate dehydrogenase complex (PDHC);

reaction arrow colored red) was increased when functional LKB1 was present in NSCLC cells. Consistent with this expected change, we observed decreased phosphorylation of acetyl-coenzyme A carboxylase (pACC) increased but increased PDHC phosphorylation in LKB1-deficient A549s (Figure 1E). This finding is consistent with a role of hypoxia inducible factor-1a (HIF-1a) in reprogramming metabolism in cells lacking functional LKB1 [5]. Computational estimation of PDHC flux and associated confidence intervals from sensitivity analyses further confirmed this finding (Figure 1F). Metabolic tracing with $[^{13}\text{C}]$ glutamine indicated there was decreased fully labeled (M+5 or M5) α KG labeling in +LKB1 cells (Figure 1G). Despite this decrease in relative glutamine anaplerosis (entry of carbon into the TCA cycle), we noted a significant increase in α KG dehydrogenase flux (Figure 1H) and increased ATP-linked respiration in +LKB1 cells. These results suggest that α KG in LKB1-deficient cells is derived directly from glutamine via glutaminase activity, whereas cells with a WT LKB1 protein obtain α KG predominantly from oxidative isocitrate dehydrogenase (IDH) flux.

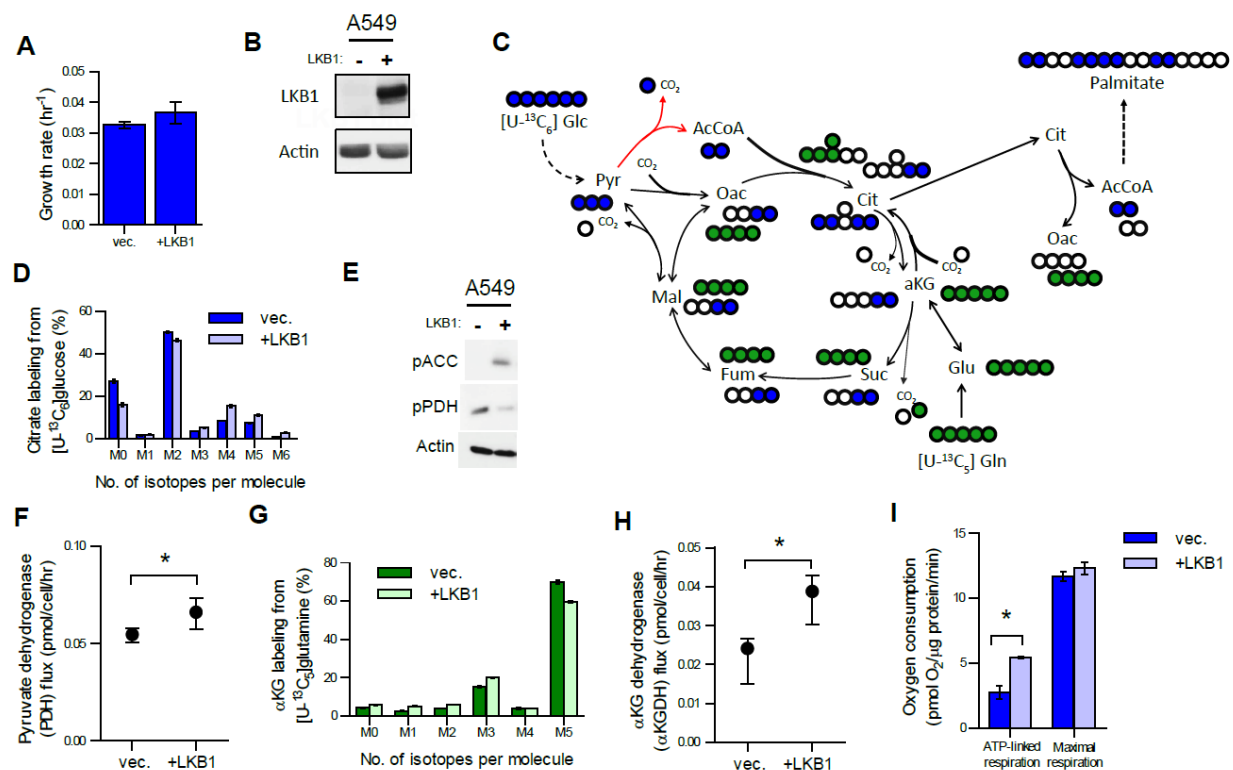


Figure 1. Metabolic regulation by the LKB1 tumor suppressor. A, B) Growth rate (A) and LKB1 expression (B) in A549 cells expressing an empty vector (vec) or functional LKB1 (+LKB1). C) Atom transition map depicting isotopic labeling downstream in the TCA cycle from $[^{13}\text{C}]$ glucose (blue) and $[^{13}\text{C}]$ glutamine (green). D) Citrate labeling from glucose. E) ACC and PDHC phosphorylation in vec. and +LKB1 cells. F) PDHC flux calculated via MFA (error bars indicates 95% confidence interval). G) α KG labeling from glutamine. H) α KGDH flux calculated via MFA (error bars indicates 95% confidence interval). I) ATP-linked or uncoupled respiration in vec. and +LKB1 cells. Error bars indicate standard deviation unless otherwise noted.

Additional MFA experiments were conducted in vec. and +LKB1 cells under conditions of metabolic stress, including hypoxia or matrix detachment. We have previously demonstrated that such conditions drive metabolic reprogramming through specific glucose and glutamine-dependent pathways [6, 7]. While NSCLC expressing or lacking LKB1 grew at similar rates under hypoxia (Figure 2A), $[13C]$ glucose tracing indicated that PDHC flux was differentially affected under this condition (Figure 2B), with +LKB1 cells maintaining higher flux through this enzyme. Nutrient/byproduct uptake and secretion were not significantly different (Figure 2C), but the extent of citrate labeling from $[13C]$ glutamine was reduced in +LKB1 cells (Figure 2D), suggesting these cells are less reliant on glutaminase activity than vec. control cells. Cells cultured on polyhydroxymethacrylate (pHEMA)-coated plates are unable to attach to matrix and undergo metabolic stress associated with decreased PDH flux [6]. Expression of functional LKB1 indicates that these cells are better able to maintain PDH flux (Figure 2E) and less reliant on glutaminase (Figure 2F) in response to such a stress. Time course analysis of AMPK, ACC, and PDH phosphorylation are consistent with these changes, as +LKB1 cells have increased pAMPK and pACC but decreased pPDH (Figure 2G). These results indicate LKB1 is critical for reprogramming cell metabolism in response to microenvironmental stress.

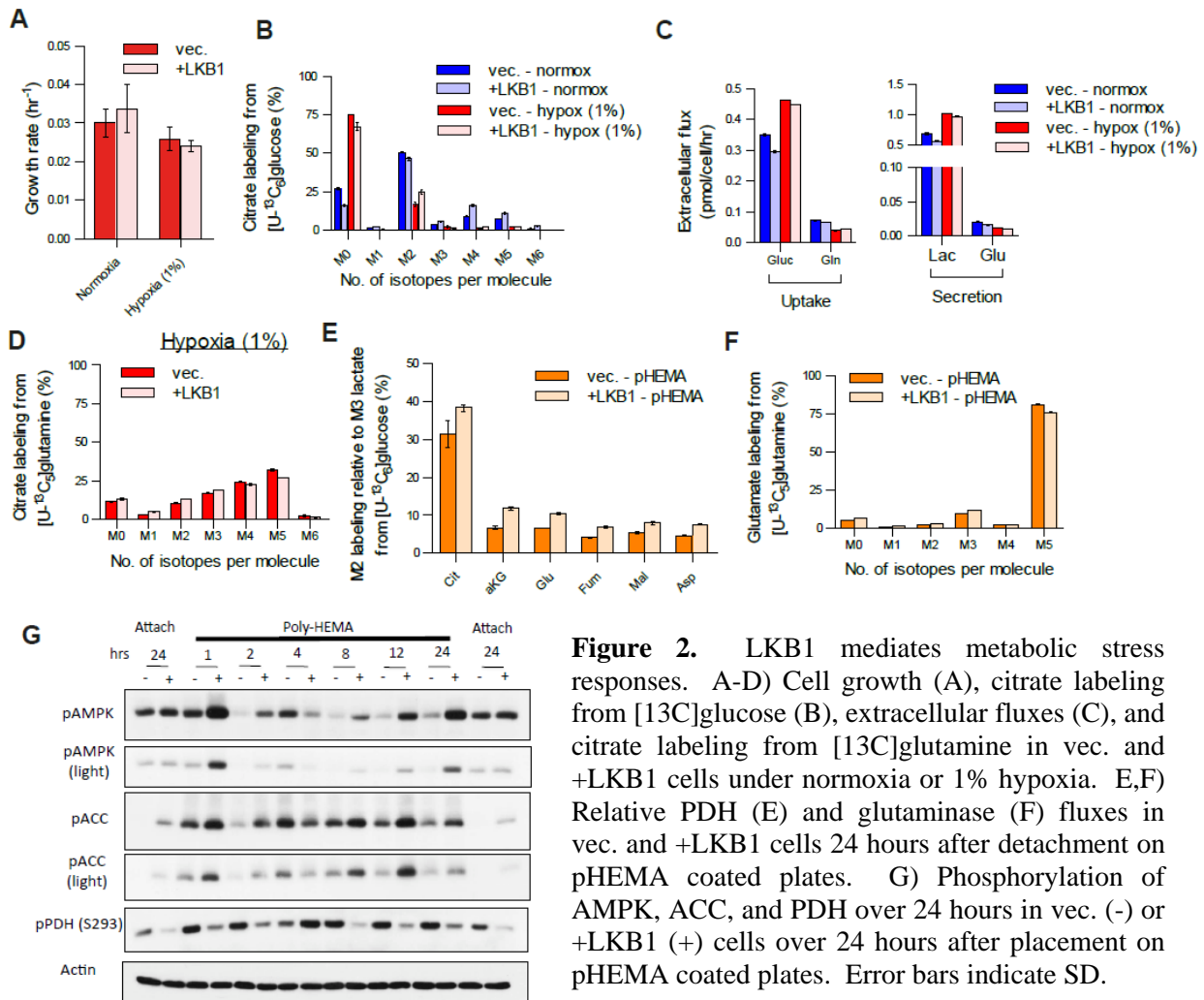


Figure 2. LKB1 mediates metabolic stress responses. A-D) Cell growth (A), citrate labeling from $[13C]$ glucose (B), extracellular fluxes (C), and citrate labeling from $[13C]$ glutamine in vec. and +LKB1 cells under normoxia or 1% hypoxia. E,F) Relative PDH (E) and glutaminase (F) fluxes in vec. and +LKB1 cells 24 hours after detachment on pHEMA coated plates. G) Phosphorylation of AMPK, ACC, and PDH over 24 hours in vec. (-) or +LKB1 (+) cells over 24 hours after placement on pHEMA coated plates. Error bars indicate SD.

Task 2. Observe the effects of biguanide treatment on NSCLC cell lines at physiologically relevant doses. NSCLC cell lines to be studied include the above A549 cells and a similar panel of H460 cells. Work to be performed by Hui Zhang and graduate student Seth Parker (months 6-10)

- 2a. Perform ^{13}C -tracing experiments above upon treating cells with decreasing doses of metformin and phenformin (months 6-10)
- 2b. Computationally resolve intracellular fluxes using the above data (months 6-10)
- 2c. Quantify cell survival in response to nutrient deprivation and hypoxia at the relevant doses of biguanides (months 6-10)

We have conducted MFA studies tracing the reliance of NSCLC cells on glutamine for AcCoA generation in response to phenformin treatment and in the context of cells that are deficient (vec.) or proficient (+LKB1) in the LKB1 tumor suppressor. $[^{13}\text{C}]$ glutamine labeling patterns indicative of oxidative glutaminolysis (blue) or reductive carboxylation (red) are depicted in Figure 3A. Phenformin drives a pronounced increase in glutaminase flux, as indicated by the extent of fully labeled (M5) glutamate from $[^{13}\text{C}]$ glutamine tracing (Figure 3B). Importantly, +LKB1 cells more proficient in synthesizing aspartate from glutamine in the presence of phenformin, as evidenced by the decreased M0 and increased M3 labeling in +LKB1+phen cells (Figure 3C). Computational MFA was conducted on palmitate labeling and demonstrated that +LKB1 cells maintained slightly higher glucose oxidation and glutamine conversion to lipids (Figure 3D), providing evidence that they are better able to survive and proliferate in the presence of phenformin. In fact, +LKB1 cells were able to proliferate (albeit at a slow rate) with 50 μM phenformin in the culture medium, whereas cells lacking functional LKB1 did not proliferate at all (Figure 3D). These results support our hypothesis that phenformin treatment and glutamine metabolism may be effective co-targets to slow LKB1-deficient tumor growth. Similar results were also observed using H460 NSCLC cells lacking or expressing functional LKB1 (not shown).

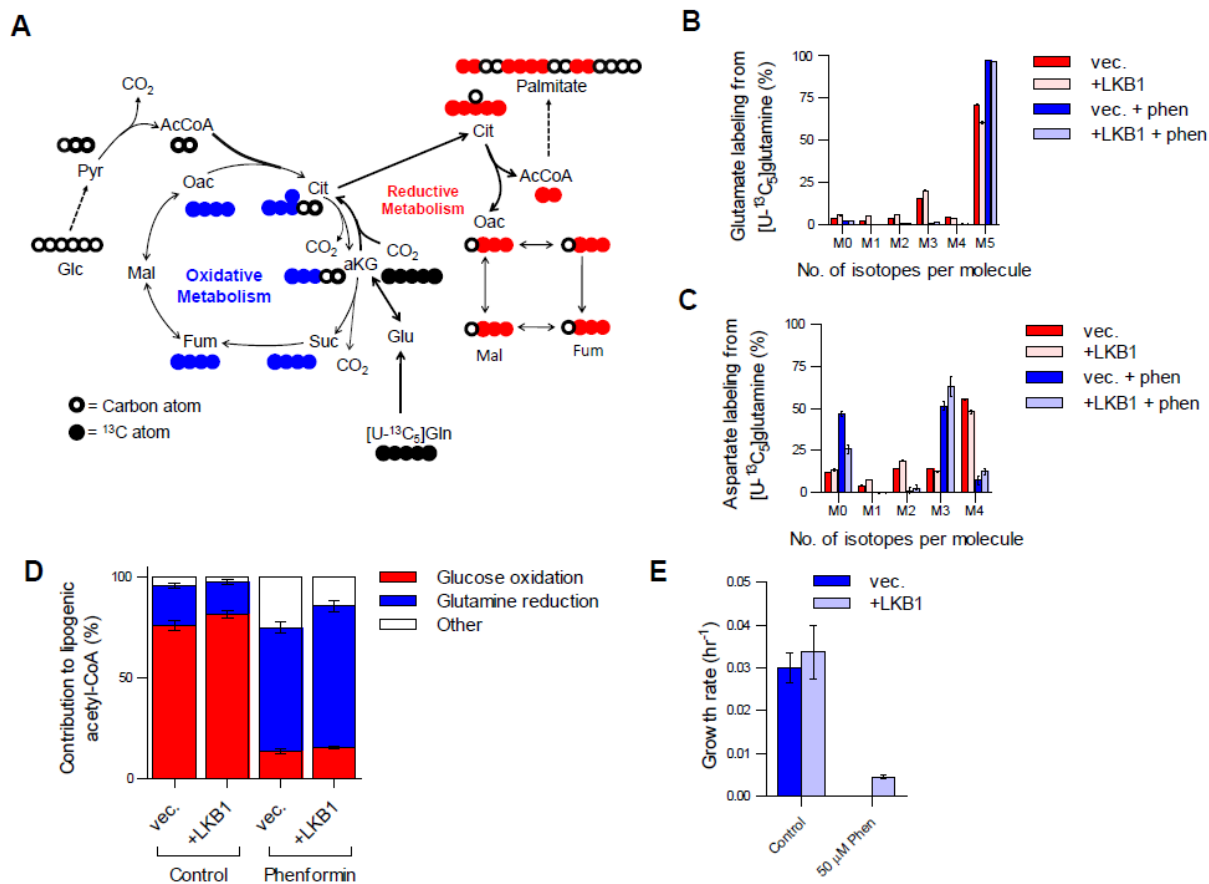


Figure 3. Phenformin reprograms glutamine metabolism. A) Atom transition map depicting oxidative (blue) and reductive (red) metabolic labeling from [13C]glutamine. B) Glutamate labeling from [13C]glutamine. C) Aspartate labeling from glutamine. D) MFA modeling quantifying the contribution of glucose and glutamine to lipid carbon (error bars indicates 95% confidence interval). E) Growth rate of vec. and +LKB1 cells in the absence or presence of 50 μM phenformin. Error bars indicate standard deviation unless otherwise noted.

Task 3. Identify the specific enzymes which catalyze glutamine anaplerosis in response to stress Work to be performed by Hui Zhang and graduate student Seth Parker (months 10-14).

- 3a. Quantitatively compare the extent of glutamine versus glutamate uptake in NSCLC cells under stress (months 10-11)
- 3b. Quantify and compare fluxes through glutaminase, nucleotide synthesis, and hexosamine synthesis using [γ-¹⁵N]glutamine to determine the enzyme(s) which convert glutamine to glutamate (months 11-12)
- 3c. Quantify and compare the flux of glutamate to a-ketoglutarate as catalyzed by aminotransferases and/or glutamate dehydrogenase using [α-¹⁵N]glutamine (months 12-13)
- 3d. Functionally validate the effects of metabolic inhibitors of each enzyme using MFA and treatments with asparaginase, 968, BPTES, azaserine, DON, aminoxyacetate, or EGCG (months 12-14).

Specific glutamine and glutamate tracing studies using [13C] and [15N] isotopes continue to be executed. Given the results in Tasks 1 and 2 that suggest glutaminase activity is elevated in LKB1-deficient NSCLC cells we have accelerated experiments that utilize inhibitors of this enzyme. BPTES and 968 are published inhibitors of glutaminase, but the former compound is a particularly good candidate, as recent studies (personal communication with Chi Dang, UPenn) indicate BPTES is much more effective at inhibiting glutaminase in culture and *in vivo*. Preliminary titration studies quantifying cell growth inhibition by BPTES indicate that vec. cells are not more sensitive to BPTES than +LKB1 cells (Figure 4). However, the sensitivity may be different in the context of phenformin treatment or within *in vivo* microenvironments, as preliminary studies that are being repeated suggest that the recovery of vec. cells in response to phenformin treatment/washout is compromised relative to +LKB1 cells and the glutaminase-dependence is exacerbated under such conditions.

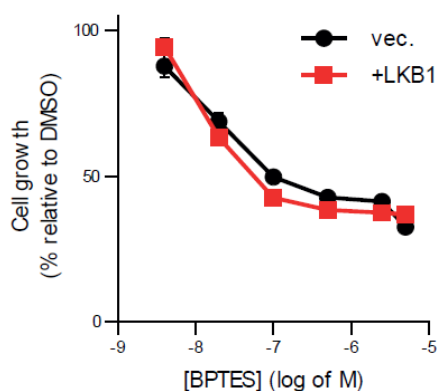


Figure 4. Cell growth inhibition by BPTES. Cells were grown in varying concentrations of the glutaminase inhibitor BPTES and quantified via plate-counting. While BPTES reduced the growth of A549 cells, under non-stress conditions no selective sensitivity was observed. Error bars indicate standard deviation.

Task 4. Evaluate the efficacy of combinatorial treatments in LKB1-proficient and deficient NSCLC cells. Work to be performed by Hui Zhang and graduate student TBN (months 14-16).

- 4a. Perform cell survival studies by treating cells with combinations of biguanides and inhibitors of glutamine metabolism (months 14-16)
- 4b. Analyze the metabolic phenotype of cells upon treatment with drug combinations (months 14-16)
- 4c. Identify the optimal target/drug to be used in combination therapy (months 15-16)

Task 5. *In vivo* testing of biguanide and glutamine metabolism inhibitors in xenograft models of LKB1-proficient and deficient NSCLC. Work to be performed by Rob Svensson at Salk and Hui Zhang and graduate student TBN

- 5a. Obtain IACUC and ACURO approval for combination therapies in xenograft mice (months 12-15)

IACUC and ACURO approval have been granted for *in vivo* xenograft studies, which will commence in the next 3 months.

- 5b. Initiate xenograft experiments with A549 cell line panel (control, WT LKB1, KD LKB1) and treat with vehicle, Gln inhibitor, phenformin, or phenformin + Gln inhibitor (months 15-19)
- 5c. Conduct xenograft/combo therapy experiments with H460 cell line panel (months 17-21)

- 5d. Evaluate the tumor burden and cell signaling profile of treated/untreated tumors through luciferase and histology analyses (months 18-23)
- 5e. Quantify metabolite profiles in plasma, tumors, and adjacent normal tissue using GC/MS analysis (months 18-24)

This grant partially supported work on related ¹³C MFA projects aimed at studying the metabolic response of cells to hypoxia in the presence or absence of mutant IDH1 and IDH2. Additional studies developed a new approach for quantifying metabolic sources of NADPH regeneration in the mitochondria and cytosol. Both of which resulted in publications [8, 9].

Key Research Accomplishments

- Identified key differences in metabolic activity in NSCLC cells lacking functional LKB1
- Demonstrated key stress conditions that exacerbate the defect caused by LKB1 loss
- Uncovered a mechanistic link between LKB1 activity and maintenance of PDH flux
- Characterized metabolic reprogramming in response to phenformin
- Explored sensitivity of LKB1-proficient and deficient cells to glutaminase inhibition under nutrient replete conditions
- Demonstrated the increased dependence of hypoxic cells on both oxidative and reductive glutamine metabolism
- Developed a tool for quantifying compartment-specific NADPH metabolism in the cytosol and mitochondria

Reportable outcomes

Research presentations:

9/2013	FSU Biochemistry Seminar, Tallahassee, FA
10/2013	Agios Pharmaceuticals MiniSymposium, Cambridge, MA
3/2014	Keystone Tumor Metabolism meeting, Whistler, Canada
3/2014	Vesalius Research Center, Leuven, Belgium
3/2014	Luxembourg Centre for Systems Biology
4/2014	AACR National Meeting
4/2014	USC Biomedical Engineering Department Seminar

Two research manuscripts were published with partial support from this grant [8, 9].

Conclusions

Our MFA results have generated a “metabolic roadmap” highlighting the distinct metabolic changes that are caused by loss of the LKB1 tumor suppressor in NSCLC. These data indicate that LKB1-deficient cells have a propensity for using glutamine to fuel bioenergetic metabolism in the TCA cycle. We have moved beyond this basic characterization and also investigated how metabolism changes in LKB1-deficient and proficient NSCLC cells when they experience stresses that affect the energy state of cells, including hypoxia, matrix detachment, and treatment with the biguanide phenformin. These studies indicate that metabolic stress further exacerbates the metabolic differences between NSCLC cells that express or lack functional LKB1. Of particular interest is the reliance of LKB1-deficient cells on flux through the glutaminase enzyme. Inhibitors are under investigation in the clinic in some cancers, and we are now exploring the efficacy of such treatments in LKB1-deficient cells. While marginal differences in

response have been observed thus far, these experiments have relied thus far on cell culture growth only. We hypothesize that the in vivo microenvironment may drive LKB1-deficient cells to be more sensitive to metabolic stress or combination treatments. Studies using xenograft models of lung tumor growth will commence in Year 2 of this grant.

Ultimately, these results can make a rapid, clinical impact by outlining specific genetic phenotypes in NSCLC that may benefit from combinatorial treatments with biguandies such as metformin (clinically used for diabetes already) or phenformin and glutaminase inhibitors. Several compounds that inhibit GLS are currently under investigation at the pre-clinical and Phase I stages (Calithera). However, metabolic treatments are likely to most effective when the specific regulatory or enzymatic defects of a given cancer are exploited as outlined here. Thus, our combinatorial therapeutic approach may provide a more efficacious means of exploiting cancer metabolism.

References

1. DeBerardinis, R.J., et al., *The biology of cancer: metabolic reprogramming fuels cell growth and proliferation*. Cell Metab, 2008. **7**(1): p. 11-20.
2. Vander Heiden, M.G., L.C. Cantley, and C.B. Thompson, *Understanding the Warburg effect: the metabolic requirements of cell proliferation*. Science, 2009. **324**(5930): p. 1029-33.
3. Shackelford, D.B. and R.J. Shaw, *The LKB1-AMPK pathway: metabolism and growth control in tumour suppression*. Nat Rev Cancer, 2009. **9**(8): p. 563-75.
4. Zamboni, N., *(13)C metabolic flux analysis in complex systems*. Curr Opin Biotechnol, 2010.
5. Shackelford, D.B., et al., *mTOR and HIF-1alpha-mediated tumor metabolism in an LKB1 mouse model of Peutz-Jeghers syndrome*. Proc Natl Acad Sci U S A, 2009. **106**(27): p. 11137-42.
6. Grassian, A.R., et al., *Erk regulation of pyruvate dehydrogenase flux through PDK4 modulates cell proliferation*. Genes Dev, 2011. **25**(16): p. 1716-33.
7. Metallo, C.M., et al., *Reductive glutamine metabolism by IDH1 mediates lipogenesis under hypoxia*. Nature, 2012. **481**(7381): p. 380-4.
8. Lewis, C.A., et al., *Tracing Compartmentalized NADPH Metabolism in the Cytosol and Mitochondria of Mammalian Cells*. Mol Cell, 2014.
9. Grassian, A.R., et al., *IDH1 Mutations Alter Citric Acid Cycle Metabolism and Increase Dependence on Oxidative Mitochondrial Metabolism*. Cancer Res, 2014. **74**(12): p. 3317-31.

Tracing Compartmentalized NADPH Metabolism in the Cytosol and Mitochondria of Mammalian Cells

Caroline A. Lewis,^{1,5} Seth J. Parker,^{2,5} Brian P. Fiske,¹ Douglas McCloskey,² Dan Y. Gui,¹ Courtney R. Green,² Natalie I. Vokes,¹ Adam M. Feist,² Matthew G. Vander Heiden,^{1,3,*} and Christian M. Metallo^{2,4,*}

¹The Koch Institute for Integrative Cancer Research at Massachusetts Institute of Technology, Cambridge, MA 02139, USA

²Department of Bioengineering, University of California, San Diego, La Jolla, CA 92093, USA

³Dana-Farber Cancer Institute, Boston, MA 02115, USA

⁴Institute of Engineering and Medicine, University of California, San Diego, La Jolla, CA 92093, USA

⁵These authors contributed equally to this work

*Correspondence: mvh@mit.edu (M.G.V.H.), cmetallo@ucsd.edu (C.M.M.)

<http://dx.doi.org/10.1016/j.molcel.2014.05.008>

SUMMARY

Eukaryotic cells compartmentalize biochemical processes in different organelles, often relying on metabolic cycles to shuttle reducing equivalents across intracellular membranes. NADPH serves as the electron carrier for the maintenance of redox homeostasis and reductive biosynthesis, with separate cytosolic and mitochondrial pools providing reducing power in each respective location. This cellular organization is critical for numerous functions but complicates analysis of metabolic pathways using available methods. Here we develop an approach to resolve NADP(H)-dependent pathways present within both the cytosol and the mitochondria. By tracing hydrogen in compartmentalized reactions that use NADPH as a cofactor, including the production of 2-hydroxyglutarate by mutant isocitrate dehydrogenase enzymes, we can observe metabolic pathway activity in these distinct cellular compartments. Using this system we determine the direction of serine/glycine interconversion within the mitochondria and cytosol, highlighting the ability of this approach to resolve compartmentalized reactions in intact cells.

INTRODUCTION

One of the defining characteristics of eukaryotic cell metabolism is the compartmentalization of reactions in different organelles. Although coordination of metabolic flux across organelles is critical for cell physiology, the inability to distinctly observe identical reactions present in more than one subcellular location has been a major barrier to understanding cell metabolism. Many of these compartmentalized reactions are oxidation/reduction (redox) reactions that utilize pyridine nucleotide-based cofactors to transfer electrons between metabolites to support biosynthesis, redox homeostasis, signal transduction, and ATP generation (Pollak et al., 2007a). For instance, reduction of NAD⁺ to NADH

captures energy from catabolic reactions to drive ATP synthesis through mitochondrial oxidative phosphorylation, while NADPH is regenerated via a different set of reactions to maintain reduced glutathione (GSH) pools and support reductive biosynthesis (Lunt and Vander Heiden, 2011). As such, NADPH has been hypothesized to be limiting for proliferation, lipid biosynthesis, and survival in response to cell stress (Diehn et al., 2009; Jeon et al., 2012; Jiang et al., 2013; Schafer et al., 2009). These compartmentalized metabolic processes impact numerous cell and tissue functions; therefore, understanding how biochemical networks function across compartments is necessary to determine how metabolism contributes to disease pathologies.

The pool of NADP(H) in cells is small relative to flux through pathways that utilize this cofactor (Pollak et al., 2007a). Thus, interconversion between the oxidized and reduced states must be coupled across all reactions involving this cofactor, and changes in abundance may not be informative for assessing the use of NADPH in a particular pathway. Neither NAD(H) nor NADP(H) is known to be transported across intracellular membranes (Nikiforov et al., 2011; Pollak et al., 2007b), and multistep shuttles involving compartmentalized redox reactions are used to transfer electrons between the mitochondria and cytosol (Bissell et al., 1976; LaNoue et al., 1974; LaNoue and Schoolwerth, 1979). This organization facilitates the maintenance of different NADPH/NADP⁺ ratios in each subcellular location and allows for the execution of compartment-specific metabolic processes. Classically, cytosolic NADPH is thought to be regenerated primarily via the oxidative pentose phosphate pathway (PPP) (Lunt and Vander Heiden, 2011; Pollak et al., 2007a). Other potential sources of cytoplasmic NADPH exist in mammalian cells, including reactions catalyzed by specific isozymes of isocitrate dehydrogenase (IDH), malic enzyme (ME), aldehyde dehydrogenase (ALDH), and methylene tetrahydrofolate dehydrogenase (MTHFD) (Pollak et al., 2007a; Tibbetts and Appling, 2010). However, isoforms of several of these enzymes also catalyze identical reactions in the mitochondria and can potentially transfer reducing equivalents between the mitochondria and the cytosol. For example, the reductive carboxylation of alpha-ketoglutarate (α KG) to isocitrate by IDH2 consumes mitochondrial NADPH, with citrate/isocitrate subsequently transported to the cytosol where it can be oxidized by IDH1 to produce cytosolic NADPH (Sazanov and Jackson, 1994; Wise et al., 2011). Theoretically,

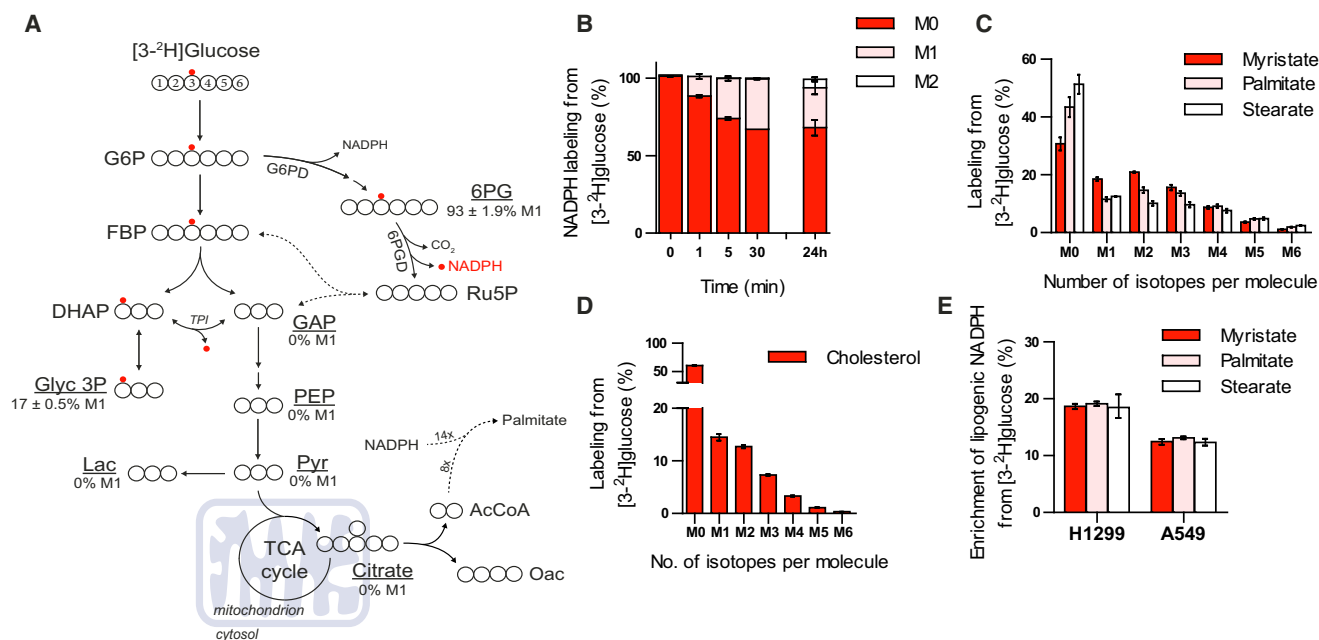


Figure 1. Use of ²H Glucose to Label Cytosolic NADPH

(A) Atom-transition map depicting a model of deuterium transfer from [3-²H]glucose through glycolysis and the pentose phosphate pathway. Open large circles represent carbon, and small red circles indicate deuterium label from [3-²H]glucose. Where measured, enrichment of M1 isotopomer (%) for glycolytic intermediates in parental H1299 cells is shown.

(B) Labeling of NADPH from [3-²H]glucose in parental H1299 cells over time.

(C) Saturated fatty acid labeling (myristate; C14:0, palmitate; C16:0 and stearate C18:0) from [3-²H]glucose in parental H1299 cells following incubation for 72 hr.

(D) Cholesterol labeling from [3-²H]glucose in parental H1299 cells cultured for 72 hr.

(E) Enrichment of lipogenic [²H]-NADPH by [3-²H]glucose estimated by a model for saturated fatty acid synthesis (ISA) in parental H1299 and A549 cells following incubation with tracer for 72 hr.

Data plotted in (A)–(D) represent mean ± SD of at least three biological replicates. For (E), data presented are mean ± 95% confidence interval of at least three biological replicates.

the reverse cycle may be used to produce mitochondrial NADPH. Metabolic cycles such as this utilize compartment-specific enzymes, and existing methods for tracing metabolism rely on breaking apart cells and pooling metabolites from all compartments, making it impossible to reliably distinguish the net reaction flux through each enzyme or pathway.

RESULTS

Tracing NADPH with ²H-Labeled Glucose

Because reaction mechanisms involving pyridine nucleotides transfer electrons as a hydride (H⁻) ion, isotope-labeled hydrogen atoms can be used to follow electron movement in these reactions (Katz et al., 1965; Rendina et al., 1984). The transfer of ²H and ³H can also be used to observe redox reactions in central carbon metabolism, an approach that has been used to generate insight into NAD(P)H metabolism in eukaryotic cells (Ben-Yoseph et al., 1994; Rühl et al., 2012). Glucose is the primary carbon source for glycolysis and the oxidative PPP in mammalian cells, with the latter pathway representing an important source of cytosolic NADPH. Nonlabile hydrogen atoms on specific glucose carbons (the 1 and 3 positions, respectively) are transferred to NADPH by the oxidative PPP enzymes

glucose-6-phosphate dehydrogenase (G6PD) and 6-phosphogluconate dehydrogenase (6PGD). The hydrogen atom on carbon-3 of glucose (which becomes carbon-1 of dihydroxyacetone phosphate in glycolysis) can exchange with water during isomerization to glyceraldehyde-3-phosphate (GAP) by triose phosphate isomerase (TPI) (Katz et al., 1965). This prevents confounding labeling of downstream metabolites including TCA cycle intermediates, suggesting that tracing this hydrogen atom could provide a means of quantifying the contribution of 6PGD to the cellular NADPH pool (Figure 1A) (Katz et al., 1966; Katz and Rognstad, 1978). To test this possibility, we cultured H1299 non-small-cell lung cancer cells in the presence of [3-²H]glucose and observed labeling of NADPH using LC/MS-MS (Figure 1B). The rapid turnover of NADPH allows labeling from [3-²H]glucose to reach isotopic steady state within 30 min, as evidenced by the lack of any increased label incorporated into NADPH after culturing cells in the presence of [3-²H]glucose for 24 hr (Figure 1B). NADPH has two hydrogens that can be transferred when it acts as an electron donor. Once labeled, either the labeled or unlabeled hydrogen atom can be transferred depending on the stereospecificity of downstream NADPH-utilizing enzymes (You, 1985). Transfer of the unlabeled hydride from labeled NADPH generates labeled NADP⁺ (see

Figure S1A available online), and subsequent labeling of the second hydrogen on NADP⁺ yields NADPH heavy by two mass units (M2) at later time points (Figure 1B). Some labeling of ribose-5-phosphate and ribulose-5-phosphate was also observed at late time points, presumably via flux through the nonoxidative PPP (Figure S1B). This label incorporation into the ribose moieties of NADP(H) could account for a minor portion of the isotope enrichment observed at 24 hr, as suggested by the small amount of M2 labeling of NADP⁺ (Figure S1A), but these atoms would not be subject to transfer in downstream reactions utilizing NADPH as a cofactor. [3-²H]glucose does not contribute to NAD(H) except by incorporation into the ribose moieties, and only a small amount of NAD(H) is labeled at late time points (Figure S1C), arguing that the majority of NADPH labeling from [3-²H]glucose reflects hydride transfer. Importantly, metabolites in lower glycolysis such as pyruvate and lactate are not labeled from [3-²H]glucose (see percent values in Figure 1A), implying that the presence of label on downstream metabolites must arise as a result of hydride transfer from labeled NADPH. [1-²H]glucose labels NADPH via G6PD in the oxidative PPP (Figures S1D and S1E), and similar to [3-²H]glucose, this label is detected on NADP⁺ and PPP intermediates (Figures S1E and S1F). However, deuterium present on carbon-1 of [1-²H]glucose can be lost due to reversibility of phosphoglucose isomerase, resulting in less glucose-6-phosphate labeling from [1-²H]glucose in cells compared to labeling from [3-²H]glucose (Figure S1G) (Ben-Yoseph et al., 1994; Hellerstein et al., 1986; Katz and Rognstad, 1976). In contrast to [3-²H]glucose, the deuterium isotope from carbon-1 of glucose does not exchange with water in any of the reactions of glycolysis and is retained on carbon entering the TCA cycle (Figure S1D). Therefore, deuterium from [1-²H]glucose has the potential to label downstream metabolites by either hydride transfer from NADPH or label retention on the carbon from glucose. As a result, use of [3-²H]glucose is preferable for tracing NADPH produced by the oxidative PPP.

The NADPH labeling we observe is a subset of the total cellular pool. To gain insights into compartment-specific redox reactions, we next quantified ²H enrichment in specific metabolites downstream of NADPH-dependent reactions. For example, fatty acid and cholesterol synthesis occur specifically in the cytosol and require NADPH. When H1299 cells are cultured with [3-²H]glucose for 72 hr to allow for accumulation of new lipid molecules, we detected significant label on newly synthesized fatty acids, including myristate (C14:0), palmitate (C16:0), and stearate (C18:0), as well as cholesterol (Figures 1C and 1D). Importantly, no label from [3-²H]glucose was detected on citrate (see percent value in Figure 1A), suggesting that isotope enrichment on lipids was from the NADPH pool that was labeled by the oxidative PPP. We also detected labeling of fatty acids from [1-²H]-glucose (Figure S1H); however, tracing of G6PD-derived NADPH is complicated by deuterium from [1-²H]glucose being retained on citrate and lipogenic acetyl-CoA (Figure S1D). We next applied isotopomer spectral analysis (ISA) to estimate the contribution of [3-²H]glucose to the lipogenic NADPH pool used for palmitate synthesis, as 14 NADPH molecules are required during the production of one palmitate molecule (Kharoubi et al., 1992; Metallo et al., 2012). The ISA model includes two parameters representing the deuterium enrichment of the

NADPH pool and the percentage of palmitate that was synthesized de novo (Figure S2). Using this method we estimated the enrichment of lipogenic NADPH from [3-²H]glucose ranged from 12%–20% in A549 and H1299 cells (Figure 1E). ISA modeling of other saturated fatty acids (e.g., myristate and stearate) yielded similar estimations for the enrichment of lipogenic NADPH from [3-²H]glucose (Figure 1E).

Use of ²H Glucose to Trace NADH Metabolism

To maintain flux through glycolysis, cytosolic NAD⁺ pools are re-generated primarily by three enzymes: lactate dehydrogenase (LDH), malate dehydrogenase (MDH), and/or the glycerol phosphate shuttle (Glyc3PDH) (Lunt and Vander Heiden, 2011; Metallo and Vander Heiden, 2013). Distinct hydrogen atoms on glucose are transferred to NAD⁺ during glycolysis via glyceraldehyde phosphate dehydrogenase (GAPDH). In theory, up to half of the hydrogen transferred to NADH via GAPDH comes from carbon four of glucose; however, exchange with water in the aldolase and TPI reactions decreases the net contribution of this hydrogen atom to NADH (Go et al., 2009) (Figure 2A). Upon culturing A549 and H1299 cells with [4-²H]glucose, significant labeling of lactate, malate, and glycerol 3-phosphate was observed (Figure 2B). Label was detected on GAP in A549 cells; however, the level of GAP in H1299 cells was below the limit of detection. In addition, no label was detected on metabolites in lower glycolysis including PEP, 3PG, and pyruvate. This pattern fits with known reactions using NADH in central carbon metabolism (Figure 2A) and suggests that [4-²H]glucose can be used to label the NADH pool produced by glycolysis in cells. Consistent with these findings, we observed rapid labeling from [4-²H]glucose on NADH (Figure 2C), as well as label on NAD⁺ (Figure S3A) arising from donation of the unlabeled hydride from M1 labeled NADH.

Interestingly, we observed isotope incorporation into fatty acid pools from [4-²H]glucose (Figure 2D), suggesting that some label from NADH transfers to cytosolic NADPH through an unknown mechanism (Figure S3F). While deuterium label from [4-²H]glucose was detected on aspartate, citrate, and isocitrate due to the symmetry of fumarate (Figures S3B–S3D), carbons labeled in this manner do not contribute to lipogenic acetyl-CoA, demonstrating that the observed fatty acid labeling is derived from hydride transferring from NAD(H) to cytosolic NADP(H). We also observed some isotope enrichment on NADP⁺ and NADPH from [4-²H]glucose (Figures 2E and S3A); however, ribose 5-phosphate and ribulose 5-phosphate are also labeled from [4-²H]glucose (Figure S3E). Furthermore, these direct measurements of total cellular NADP(H) cannot distinguish between cytosolic and mitochondrial pools, highlighting the need for methods to elucidate compartment-specific NADP(H) pools.

A Reporter System to Trace Compartmentalized Sources of NADPH

The above data demonstrate that we can observe cytosolic production of NADPH and NADH in intact cells. Although we were able to quantify the contribution of oxidative PPP enzymes to the lipogenic NADPH pool, deuterium tracing alone cannot distinguish other compartmentalized sources of

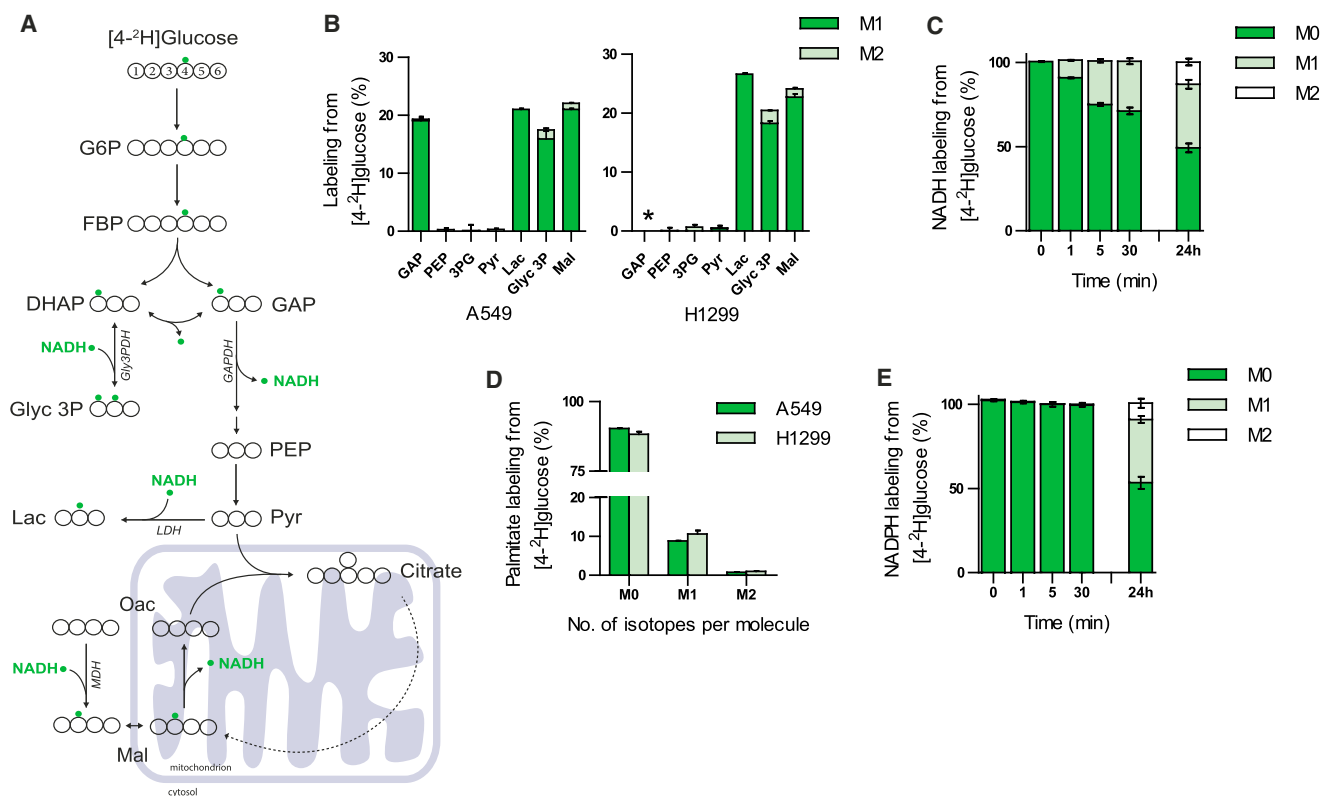


Figure 2. Use of ^2H Glucose to Label NADH

(A) Atom-transition map depicting a model of deuterium transfer from $[4-^2\text{H}]$ glucose through glycolysis and NAD^+ -dependent shuttle systems (malate dehydrogenase *MDH*, glycerol 3-phosphate dehydrogenase *Gly3PDH*, and lactate dehydrogenase *LDH*). Open large circles represent carbon, and small green circles indicate deuterium label from $[4-^2\text{H}]$ glucose.

(B) Labeling of glycolytic intermediates from $[4-^2\text{H}]$ glucose in A549 (left panel) and H1299 (right panel) cells. Glycerinaldehyde-3-phosphate (GAP) was below the limit of detection in H1299 cells, indicated by asterisk.

(C) Labeling of NADH from $[4-^2\text{H}]$ glucose in parental H1299 cells over time.

(D) Palmitate labeling from $[4-^2\text{H}]$ glucose in A549 and H1299 cells following incubation with tracer for 72 hr.

(E) Time course labeling of NADPH from $[4-^2\text{H}]$ glucose in parental H1299. Data presented are mean \pm SD of at least three biological replicates.

NADPH. Therefore, we sought to develop a reporter system that can detect pathway-specific NADPH production in different subcellular compartments. To accomplish this, we took advantage of the neomorphic mutant IDH enzymes that produce (D)2-hydroxyglutarate (2HG) from αKG . This reaction reduces αKG by transferring a hydride from NADPH to form 2HG. As 2HG is a xenometabolite that is only present at very low levels in most cells (Matsunaga et al., 2012), it can be used as an endproduct readout. By applying specific metabolic ^2H -tracers to cells and measuring enrichment of 2HG produced by ectopically expressed mutant IDH1 (cytosol) or IDH2 (mitochondria), we reasoned that pathway-specific information on NADPH metabolism in each compartment could be obtained (Figure 3A).

We generated H1299 and A549 cell lines that express epitope-tagged mutant IDH1-R132H (mtIDH1-C) or mutant IDH2-R172K (mtIDH2-M) in a doxycycline-dependent manner (Figure S4A). We employed a weak promoter to minimize effects on endogenous IDH metabolism. Indeed, FLAG-tagged mtIDH1-C was expressed at levels that were not detectable with an antibody

recognizing wild-type IDH1 enzyme in these cells (Figure S4A). mtIDH1-C is expected to be expressed in the cytoplasm and mtIDH2-M in the mitochondria, and we confirmed the localization of each using cell fractionation and western blotting (Figure 3B). We also confirmed that the FLAG-tagged mutant IDH enzymes produce 2HG in a doxycycline-dependent manner in both H1299 and A549 cell lines (Figure 3C). Interestingly, mtIDH1-C produced less 2HG than mtIDH2-M in cells, consistent with observations that ectopically expressed IDH2 mutants produce more 2HG than IDH1 mutants due to their mitochondrial localization (Ward et al., 2013). In all cases, 2HG levels were far below those observed in tumor cell lines expressing endogenous mutations in *IDH1* (R132C/+, HT1080) or *IDH2* (R172S/+, SW1353) (Figure 3D). Introduction of mutant IDH enzymes could impact NADPH or TCA metabolism; however, 2HG production flux observed in cell lines expressing IDH1 mutants at higher levels is small relative to other αKG -dependent reaction fluxes, suggesting mutant IDH expression has a minimal direct impact on αKG pools (Grassian et al., 2014). Furthermore, no significant change in $[3-^2\text{H}]$ glucose contribution to cytosolic NADPH was

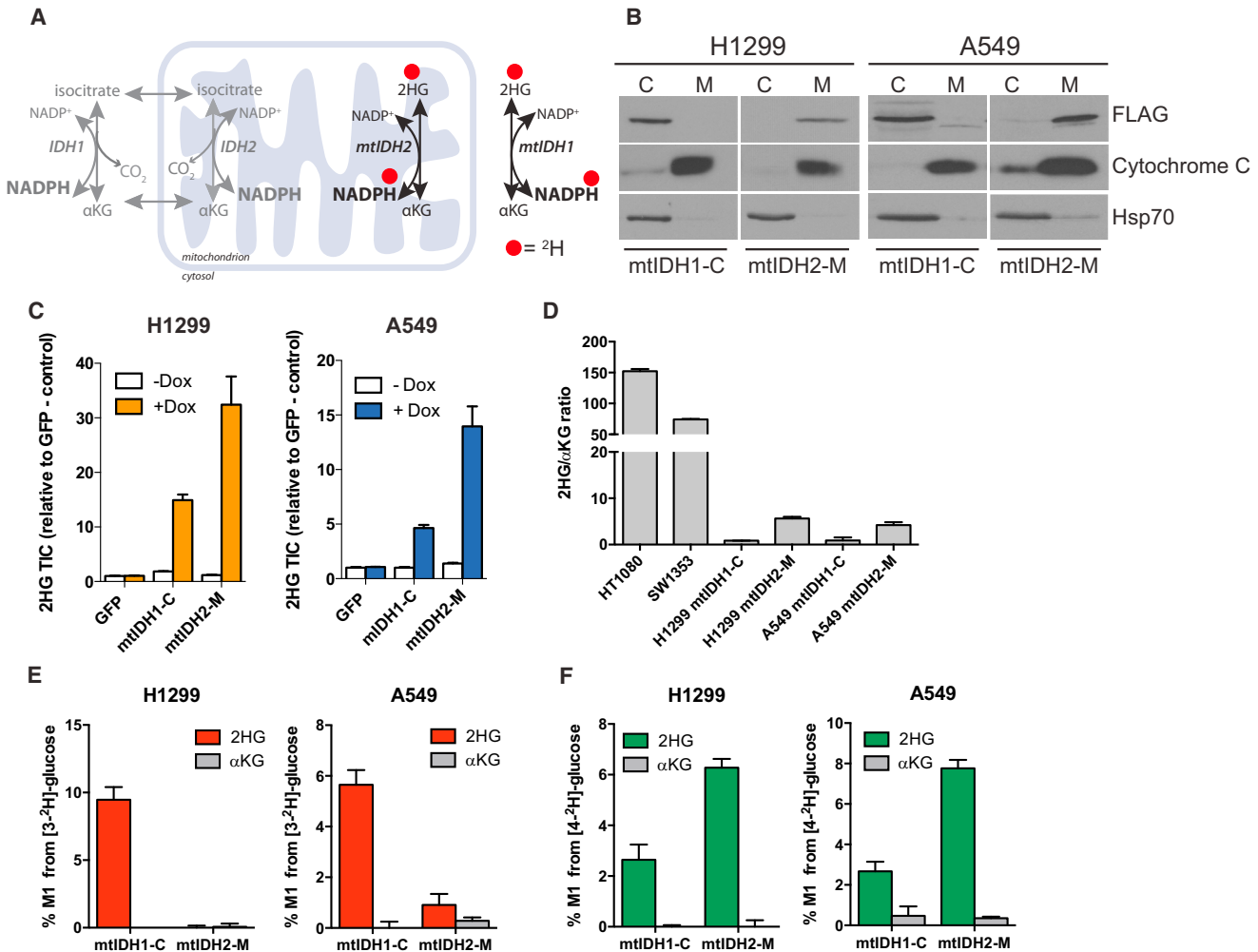


Figure 3. Generation and Characterization of Cell Lines Expressing Inducible Mutant IDH

(A) Schematic demonstrating the transfer of deuterium (red dots) from NADPH to 2HG via the reaction catalyzed by mutant IDH enzymes. mtIDH1 is localized to the cytoplasm, and mtIDH2 is localized to the mitochondria. By expressing compartment-specific mutant enzymes and combining this with deuterated glucose tracer, it is possible to track 2HG production and therefore the source of the NADPH used to make the 2HG in the cytosol or the mitochondria.

(B) Mutant IDH1-R132H is localized to the cytosol (mtIDH1-C), and mutant IDH2-R172K is localized to the mitochondria (mtIDH2-M) in H1299 and A549 cells. Cells were transduced with lentiviral constructs containing cDNA encoding C-terminal FLAG-tagged IDH1-R132H or IDH2-R172K under the control of a doxycycline (dox)-inducible promoter. Once stable cell lines were established, cells were treated with 0.1 $\mu\text{g}/\text{mL}$ dox for 24 hr. Protein expression was analyzed by cellular fractionation and western blotting using antibodies against FLAG, cytochrome c (mitochondrial-specific marker), and Hsp70 (cytoplasmic-specific marker). C, Supernatant-100 fraction (cytoplasm); M, mitochondria. Samples from mtIDH1-C and mtIDH2-M cells were analyzed on separate gels.

(C) Cell lines expressing inducible IDH mutants produce 2HG in a dox-dependent manner. H1299 and A549 cells stably expressing inducible mtIDH1-C or mtIDH2-M constructs were treated with doxycycline (0.1 $\mu\text{g}/\text{mL}$) for 24 hr. Amounts of 2HG (total ion counts, TIC) are shown relative to GFP control cells treated with vehicle.

(D) 2HG production, as measured by 2HG/ αKG ratio, is much higher in cell lines harboring endogenous mutations in *IDH1* (R132C/+, HT1080) and *IDH2* (R172S/+, SW1353) than cells expressing mtIDH1-C and mtIDH2-M.

(E) NADPH produced by the pentose phosphate pathway (6PGD) is cytosolic. Cells were cultured in [3- ^2H]-glucose (10 mM) for 24 hr before adding dox (0.1 $\mu\text{g}/\text{mL}$) for 24 hr to induce mutant IDH expression, and amount of M1 label (%) from [3- ^2H]-glucose incorporated into 2HG and αKG was measured.

(F) NADH supports NADPH production in the mitochondria. Cells were incubated with 10 mM [4- ^2H]-glucose for 24 hr and treated and analyzed as in E. Data represent mean \pm SEM of at least three biological replicates.

observed in A549 cells following mtIDH1-C or mtIDH2-M expression (Figure S4G).

Although doxycycline can affect the metabolism and proliferation of some mammalian cancer cell lines in culture (Ahler et al., 2013), we saw no doxycycline-dependent changes in the

abundance of central carbon metabolites (Figure S4B) or in the proliferation rate (Figure S4C) of A549 or H1299 cells. Importantly, cells expressing doxycycline-inducible GFP also showed no changes in metabolite pool sizes or proliferation rates (Figures S4B and S4C), indicating that when added at this concentration

doxycycline does not significantly affect metabolism in this system. In addition, we observed no significant differences in pool sizes of NAD⁺, NADH, NADP⁺, or NADPH in H1299 mtIDH1-C and mtIDH2-M cells following the addition of doxycycline for 24 hr, suggesting that doxycycline-dependent production of 2HG was not altering the availability of these cofactors for use in other redox reactions (Figure S4D). This is supported by the reported k_{cat} of mutant IDH1 enzymes being small relative to wild-type IDH1 (Dang et al., 2009) and suggests that any direct effects of these enzymes on cellular redox state are minimal.

Validation of Compartment-Specific Cofactor Tracing

To validate the ability of this system to trace compartment-specific NADPH metabolism, we induced expression of the mutant IDH enzymes in cells cultured in the presence of [3-²H]glucose and measured enrichment of ²H in the 2HG pool. In order to ensure that the cells were at or near isotopic steady state prior to induction of mutant IDH expression, the cells were incubated with tracer for 24 hr prior to the addition of doxycycline. Consistent with [3-²H]glucose producing cytosolic NADPH via the oxidative PPP, 2HG was only significantly labeled from [3-²H]glucose in the mtIDH1-C cell lines and not in the mtIDH2-M cell lines (Figure 3E). Importantly, little to no label was observed on α KG under these conditions, ensuring that label on 2HG was a direct result of hydride ion transfer from NADPH by the mutant enzyme. We next asked whether label from [4-²H]glucose was incorporated into 2HG by either mtIDH1-C or mtIDH2-M. Notably, more 2HG was labeled from [4-²H]glucose in mtIDH2-M cells than in mtIDH1-C cells (Figure 3F). These data suggest that transfer of H⁻ from NADH to NADPH occurs through a mitochondrial intermediate (e.g., malate) or via nicotinamide nucleotide transhydrogenase (NNT), and transfer of reducing equivalents from NADH to NADPH mostly supports the mitochondrial NADPH pool. Similar results were observed in cell lines with endogenous, heterozygous *IDH1* and *IDH2* mutations (Figures S4E and S4F).

In vitro steady-state enzyme kinetics experiments have demonstrated that rate constants for reactions involving ²H transfer can be lower compared to studies conducted with unlabeled substrate (Rendina et al., 1984). This phenomenon has been an invaluable tool for elucidating biochemical reaction mechanisms, including many of the reactions responsible for label transfer in our system. However, given the diverse means through which metabolism is regulated and the challenges associated with understanding which enzymatic steps are rate limiting for pathways in intact cells, the relevance of isotope effects to intracellular metabolic fluxes is not clear. To determine the significance of this phenomenon in our system, we cultured cells in different ratios of [3-²H]glucose and unlabeled glucose and measured downstream labeling of lipogenic NADPH and 2HG in H1299 mtIDH1-C cells (Figure 4A). Similarly, we titrated [4-²H]glucose with unlabeled substrate in H1299 mtIDH2-M cells and observed whether label transfer to lactate, malate, aspartate, fumarate, citrate, and 2HG was affected by different amounts of labeled substrate (Figure 4B). We reasoned that if reaction rates are affected by the presence of ²H isotopes, the use of unlabeled substrates would be favored and less relative transfer of label would be observed as unlabeled substrate is

titrated into the medium. However, in all cases, transfer of label from either tracer decreased linearly as the tracer was diluted with unlabeled substrate, suggesting that kinetic isotope effects minimally impact the results of these experiments (Figures 4A and 4B). A linear decrease in lipogenic NADPH and 2HG labeling was also observed in endogenous mtIDH1 cells (HT1080) that exhibit much higher rates of 2HG production when we titrated [3-²H]glucose, further supporting the notion that isotope effects minimally affect substrate fluxes through the reactions we traced in intact cells (Figure 4C).

Characterizing Serine/Glycine Metabolism in the Cytosol and Mitochondria

We next sought to use our reporter system to examine a compartmentalized metabolic cycle. Reactions that make up folate-mediated one-carbon metabolism exist in both the cytosol and the mitochondria, although it is not clear from current literature whether these are linked in a cycle and/or in which direction the reactions proceed (Anderson et al., 2011; Nilsson et al., 2014; Tedeschi et al., 2013; Tibbetts and Appling, 2010). Serine and glycine interconversion via serine hydroxymethyltransferase (SHMT) has been observed in cultured cells (Jain et al., 2012; Levintow and Eagle, 1961; Perry et al., 2007), but ¹³C tracing is unable to ascertain the directionality, compartmentalization, and interconnectivity of this process. Indeed, upon culture with [U-¹³C₃]serine, we observed significant interconversion of serine and glycine in A549 mtIDH1-C and mtIDH2-M cells (Figure 5A). The reactions catalyzed by MTHFD1 (cytosolic) and MTHFD2/MTHFD2L (mitochondrial) utilize NAD(P)H (Figure 5B); therefore, we hypothesized that ²H serine and glycine tracing in combination with our compartment reporter system would enable us to experimentally determine the direction of serine-glycine exchange reactions in the cytosol and mitochondria. Hydrogens on carbon-3 of serine are transferred to 5,10-methylenetetrahydrofolate (5,10-methyleneTHF) and subsequently to NADPH via MTHFD1/2 (Figure 5B). Additionally, the glycine cleavage system (GCS) exists in the mitochondria and could transfer hydrogen from carbon two of glycine to 5,10-methylene-THF and generate NADPH (Figure 5B) (Kikuchi et al., 2008).

To study these compartment-specific pathways, we cultured A549 mtIDH1-C and mtIDH2-M cells with either [3,3-²H₂]serine or [2,3,3-²H₃]serine and unlabeled glycine or [2,2-²H₂]glycine and unlabeled serine and measured incorporation of ²H in cytosolic or mitochondrial 2HG, respectively. Strikingly, we detected label from [3,3-²H₂]serine and [2,3,3-²H₃]serine on 2HG only in mtIDH2-M cells, strongly suggesting that serine to glycine conversion occurs primarily in the mitochondria in these cells with the MTHFD2/MTHFD2L reaction operating oxidatively (Figures 5C and S5A–S5C). We did not observe labeling of 2HG from [2,2-²H₂]glycine in cells expressing either mutant IDH (Figure 5C), indicating that either the majority of mitochondrial glycine is generated by SHMT2 (rather than glycine import) or the label is lost in the GCS. Consistent with the lack of label transfer from ²H-labeled serine or glycine to 2HG in mtIDH1-C cells, we detected minimal contribution of these tracers in the lipogenic NADPH pool (Figure 5D). To further confirm the direction of MTHFD1, we cultured A549 mtIDH1-C and mtIDH2-M cells with [3-²H]glucose, which specifically labels cytosolic NADPH.

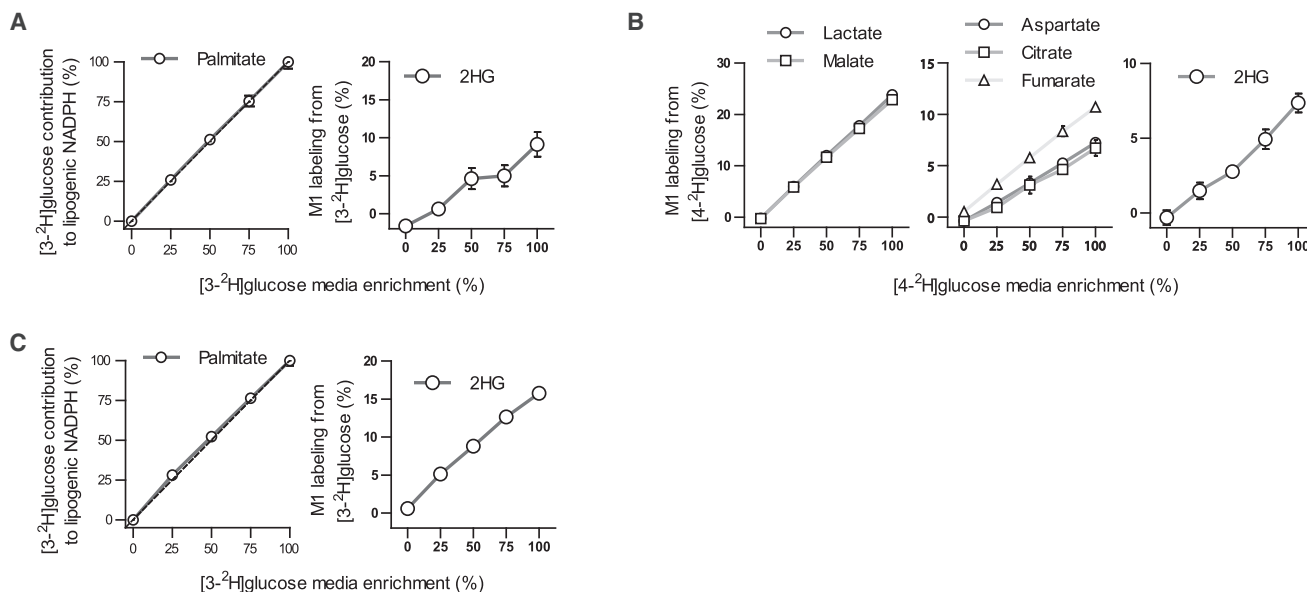


Figure 4. Kinetic Isotope Effect Minimally Affects [3-²H]Glucose and [4-²H]Glucose Metabolism

(A) [3-²H]glucose was titrated with unlabeled glucose and added to H1299 cells expressing mtIDH1-C. Contribution from [3-²H]glucose to lipogenic NADPH (left panel, normalized to contribution at 100% [3-²H]glucose media enrichment) and 2HG (right panel) was measured. Dashed line (left panel) represents 1:1 contribution of [3-²H]glucose to lipogenic NADPH to enrichment of [3-²H]glucose in media.

(B) [4-²H]glucose was titrated with unlabeled glucose and added to H1299 cells expressing mtIDH2-M. Labeling from [4-²H]glucose on lactate and malate (left panel); aspartate, citrate, and fumarate (middle panel); and 2HG (right panel) was measured.

(C) [3-²H]glucose was titrated with unlabeled glucose in HT1080 cells harboring endogenous *IDH1* mutations (R132C/+). Contribution from [3-²H]glucose to lipogenic NADPH (left panel, normalized to contribution at 100% [3-²H]glucose media enrichment) and M1 labeling on 2HG (right panel) was quantified at 0%, 25%, 50%, 75%, and 100% dilution with unlabeled glucose (left panel) in HT1080 cells cultured with [3-²H]glucose diluted with unlabeled glucose at 0%, 25%, 50%, 75%, and 100% enrichment.

Data presented are shown as mean ± SD of three biological replicates for (A) (right panel), (B), and (C) (right panel). Data represent mean ± 95% confidence interval for at least three biological replicates for (A) (left panel) and (C) (left panel).

We observed transfer of ²H from [3-²H]glucose onto serine, suggesting that cytosolic MTHFD1 can operate in the reductive direction in these cells (Figure 5E). The lack of glycine labeling from [3-²H]glucose confirms label transfer to serine was obtained from 5,10-methyleneTHF (Figures 5E and S5D). The lack of labeling from either [2,3,3-²H₃]serine or [3,3-²H₂]serine on either fatty acids or 2HG produced by mtIDH1-C is also consistent with minimal contribution of MTHFD1 to the cytoplasmic NADPH pool in these cells, although channeling to other reactions cannot be ruled out by these methods. Shuttling of serine labeled by [3-²H]glucose by MTHFD1/SHMT1 into the mitochondria for catabolism by MTHFD2/SHMT2 may account for the small amount of label (<1%) we observe on mitochondrial 2HG in A549 mtIDH2-M cells cultured with [3-²H]glucose (Figure 3E). Collectively, these data provide direct evidence that serine metabolism can contribute to regenerating mitochondrial NADPH in cells.

DISCUSSION

We have developed a system that can distinguish compartmentalized pools of NADPH, demonstrating the directionality and interconnectivity of serine/glycine metabolism in the cytosol and mitochondria of intact cells. In the cells studied, conversion of serine to glycine occurs primarily in the mitochondria with

the reaction catalyzed by MTHFD2/MTHFD2L contributing to NADPH production in this compartment. Interestingly, label transfer from both [2,3,3-²H₃]serine and [3,3-²H₂]serine to mitochondrial 2HG was observed, suggesting that serine metabolism by SHMT2 is a contributor to the mitochondrial NADPH and glycine pools. These data also provide direct experimental support for the hypothesis that the cytoplasmic source of formate used for purine synthesis can be mitochondrially derived in some cells. Previous efforts to ascertain directionality of folate-mediated one-carbon metabolism have been unable to distinguish between compartments, relying on expression data (Nilsson et al., 2014), mathematical modeling (Scotti et al., 2013; Tedeschi et al., 2013), or isolated mitochondrial preparations (Barlowe and Appling, 1988). The importance of distinguishing compartmentalized redox pathways is highlighted by the large number of potential pathways that have been implicated in the shuttling of reducing equivalents between the cytosol and mitochondria. For instance, compartment-specific metabolic cycling through citrate/αKG (Sazanov and Jackson, 1994; Ward et al., 2010), malate/pyruvate (Jiang et al., 2013; Son et al., 2013), proline (Hagedorn and Phang, 1983; Nilsson et al., 2014), and serine (Tibbetts and Appling, 2010) have been suggested to be important for mammalian cell physiology. Although carbon tracing is increasingly combined with genetic approaches to implicate a role for compartment-specific

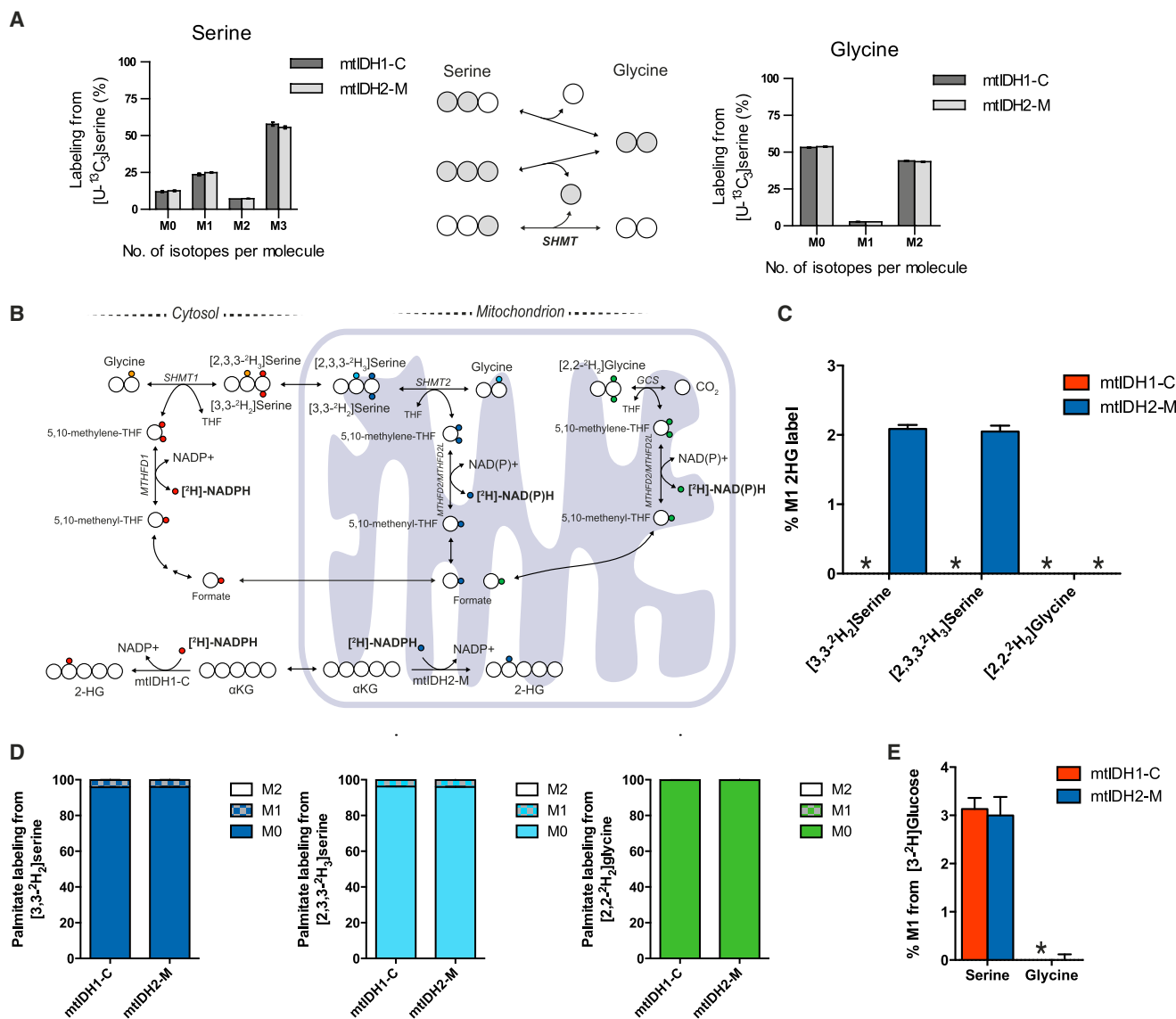


Figure 5. Characterizing Serine/Glycine Metabolism in the Cytosol/Mitochondria

(A) Serine (left panel) and glycine (right panel) labeling in A549 mtIDH1-C and mtIDH2-M cells cultured with [U-¹³C₃]serine. Cells were incubated with [U-¹³C₃]serine for 24 hr prior to dox-induction (0.1 μg/mL) for an additional 48 hr. Middle panel demonstrates interconversion of serine and glycine by SHMT. Data plotted represent mean ± SD for three biological replicates.

(B) A schematic of folate-mediated one-carbon metabolism in cytosolic and mitochondrial compartments catalyzed via SHMT and MTHFD. Deuterium transfer from [3,3-²H₂]serine is shown for pathways containing SHMT and MTHFD and is indicated by small red or blue circles for cytosolic and mitochondrial isozymes, respectively. The extra deuterium on [2,3,3-²H₃]serine is indicated by an orange (cytosolic) or a turquoise (mitochondrial) circle. Deuterium transfer from [2,2-²H₂]glycine is shown for the glycine cleavage system (GCS) pathway indicated by small green circles.

(C) 2HG labeling from [3,3-²H₂]serine, [2,3,3-²H₃]serine or [2,2-²H₂]glycine in A549 mtIDH1-C and mtIDH2-M cells. Cells were incubated with either tracer for 24 hr prior to dox induction (0.1 μg/mL) for an additional 48 hr. No label was detected on 2HG in mtIDH1-C cells from either [3,3-²H₂]serine or [2,3,3-²H₃]serine, nor was label detected on 2HG from [2,2-²H₂]glycine in mtIDH1-C and mtIDH2-M cells (indicated by asterisk).

(D) Fatty acid labeling from A549 mtIDH1-C and mtIDH2-M cells cultured with either [3,3-²H₂]serine, [2,3,3-²H₃]serine, or [2,2-²H₂]glycine. Cells were incubated with tracer for 24 hr prior to dox induction (0.1 μg/mL) for an additional 48 hr.

(E) Serine and glycine labeling in A549 mtIDH1-C and mtIDH2-M cells cultured with [3-²H]glucose. Cells were incubated with tracer for 24 hr prior to dox induction (0.1 μg/mL) for 48 hr. Data represent mean ± SEM of at least three biological replicates.

isozymes in such processes, adaptation to genetic depletion strategies that break these cycles can confound interpretation. The reporter system described here circumvents these issues

for reactions involving NADPH by providing direct visualization of compartmentalized reaction activity and direction in intact cells.

Other subcellular compartments also have distinct metabolic needs in eukaryotic cells and could be probed with an analogous approach by engineering the localization of mutant IDH enzymes and/or monitoring ^2H transfer between other metabolites. The endoplasmic reticulum (ER) is an important site for protein folding, disulfide bond formation, long chain fatty acid extension, and sterol reduction; as such, the $\text{NADP}^+/\text{NADPH}$ ratio within the ER can influence diverse cellular and physiological processes (Bánhegyi et al., 2009; Kardon et al., 2008; Száraz et al., 2010). This approach may also be adapted to quantify the $\text{NADP}^+/\text{NADPH}$ ratio in particular organelles and the turnover rate of NADPH in specific compartments. Altering the cofactor selectivity of the mutant IDH enzyme, or relying on NADH-dependent production of another xenometabolite could similarly be used to visualize compartmentalized reactions that utilize NADH. Finally, these data may be integrated with compartmentalized ^{13}C metabolic flux analysis (MFA) models to better understand the role of cofactor metabolism in metabolic engineering applications or disease models (Rühl et al., 2012). Thus, this approach opens up new avenues to observe metabolic processes in complex cells and improve our understanding of metabolism in normal and disease states.

EXPERIMENTAL PROCEDURES

Cell Culture and Isotopic Labeling

All cell lines were maintained in DMEM supplemented with 10% FBS, 100 U/mL penicillin/streptomycin, and 4 mM L-glutamine. The pSLIK-mtIDH cell lines (see below) were maintained as above, but FBS was substituted for Tet-free FBS (Clontech). Cell number was determined using an automated cell counter (Nexcelom) or by haemocytometer. For isotopic labeling experiments in the pSLIK-mtIDH cell lines, cells were cultured in 6-well plates in glucose- and glutamine-free DMEM, supplemented with 10% dialyzed Tet-free FBS, 100 U/mL penicillin/streptomycin, 4 mM L-glutamine, and 10 or 15 mM of the appropriate deuterated glucose tracer ($[3\text{-}^2\text{H}]$, 95% or 98%]glucose or $[4\text{-}^2\text{H}]$, 94% or 98%]glucose) for 24 hr or 48–72 hr incubation, respectively (Omicron and Cambridge Isotope Laboratories, Inc.). For cholesterol labeling experiments, parental H1299 cells were cultured in DMEM supplemented with 1% FBS for two passages prior to 72 hr incubation with $[3\text{-}^2\text{H}]$ glucose. Cells were cultured in tracer medium for 24 hr prior to the addition of doxycycline hyclate (0.1 $\mu\text{g}/\text{mL}$ in water; Sigma) for 24–48 hr in order to induce mutant IDH expression and accumulate 2HG. Isotope-labeled glycine and serine tracer medium was prepared from custom phenol red-, glucose-, sodium pyruvate-, amino acid-, and sodium bicarbonate-free DMEM (Hyclone Laboratories, Inc.) supplemented with 10% dialyzed Tet-free FBS, 3.7 g/L sodium bicarbonate, and DMEM-levels of L-arginine, L-cystine, L-glutamine, L-histidine, L-isoleucine, L-leucine, L-lysine, L-methionine, L-phenylalanine, L-threonine, L-tryptophan, L-tyrosine, and L-valine prepared as a 100 \times stock in aqueous acid (pH 2.0). A549 pSLIK mtIDH1-C and mtIDH2-M cells were cultured in serine- and glycine-free DMEM supplemented with either $[2,3,3\text{-}^2\text{H}_3]$, 98%]serine or $[3,3\text{-}^2\text{H}_2]$, 98%]serine and unlabeled glycine (0.4 mM) (Cambridge Isotope Laboratories, Inc.), or $[2,2\text{-}^2\text{H}_2]$, 98%]glycine and unlabeled serine (0.4 mM) (Cambridge Isotope Laboratories, Inc.). Cells were cultured in the presence of tracer medium for 24 hr prior to doxycycline addition (0.1 $\mu\text{g}/\text{mL}$) for a further 48 hr.

Generation of Cell Lines Stably Expressing Inducible Forms of FLAG-Tagged Mutant IDH

To generate the doxycycline-inducible mutant IDH (mtIDH) cell lines, full-length cDNA for *IDH1-R132H* and *IDH2-R172K* was amplified by PCR and cloned into the p3xFLAG-CMV14 vector (Sigma) to generate C-terminal FLAG-tagged constructs. cDNA for *IDH1-R132H-FLAG* and *IDH2-R172K-FLAG* was then amplified by PCR and cloned into the pEN₃TTmcs entry vector

for recombination into the pSLIK-hygro lentiviral vector (both vectors from Addgene [Shin et al., 2006]). Lentiviruses were produced by transfecting HEK293T cells with the pSLIK-hygro-IDH1-R132H or pSLIK-hygro-IDH2-R172K plasmids along with the lentiviral packaging plasmids pMDLg/pRRE and pRSV-Rev and the envelope plasmid pMD2.G (all from Addgene). Supernatants containing lentiviral particles were collected 48 hr after transfection and used to infect subconfluent H1299 and A549 cells. Infected cells were allowed to recover for 24 hr before being placed under selection with 350 $\mu\text{g}/\text{mL}$ hygromycin (Invitrogen) for 10 days. Protein expression was induced using 0.1 $\mu\text{g}/\text{mL}$ doxycycline hyclate (Sigma) for 24–48 hr.

Protein Expression Analysis and Cellular Fractionation

For whole-cell extracts, cells were lysed in RIPA buffer. Mitochondrial and cytoplasmic fractions were prepared as previously described (Vander Heiden et al., 1997). Briefly, cells were harvested in buffer A (250 mM sucrose, 20 mM HEPES, 10 mM KCl, 1.5 mM MgCl_2 , 1 mM EDTA, 1 mM EGTA, 1 mM DTT, 1 \times EDTA-free protease inhibitor cocktail tablet (Roche) [pH 7.4]) and broken apart using a mechanical homogenizer (H & Y Enterprise, Redwood City, CA). Following centrifugation at 750 \times g to remove unlysed cells and nuclei, mitochondria were isolated by centrifuging at 10,000 \times g for 25 min. The resulting pellet was resuspended in buffer A and represents the mitochondrial fraction. The remaining supernatant containing cytoplasmic and membrane proteins was centrifuged for 1 hr at 100,000 \times g. The supernatant from this final spin represents the S100 fraction. Protein expression was analyzed by western blotting using antibodies against FLAG (DYKDDDDK tag, Cell Signaling), IDH1 (Santa Cruz), IDH2 (Abcam), Cytochrome C (clone 7H8.2C12, Abcam), Hsp 70 (Cell Signaling).

Metabolite Extraction and GC-MS Analysis

Polar metabolites and fatty acids were extracted using methanol/water/chloroform as previously described (Metallo et al., 2012). Parental and pSLIK-mtIDH cells were cultured in 6-well or 12-well plates, and volumes of tracer media and extraction buffers were adjusted accordingly. Derivatization of both polar metabolites and fatty acids has been described previously (Metallo et al., 2012). Briefly, polar metabolites were derivatized to form methoxime-tBDMs derivatives by incubation with 2% methoxylamine hydrochloride (MP Biomedicals) in pyridine (or MOX reagent (Thermo Scientific) followed by addition of N-tert-butyltrimethylsilyl-N-methyltrifluoroacetamide (MTBSTFA) with 1% tert-butyltrimethylchlorosilane (t-BDMCS) (Regis Technologies). Nonpolar fractions, including triacylglycerides and phospholipids, were saponified to free fatty acids and esterified to form fatty acid methyl esters by incubation with 2% H_2SO_4 in methanol. Derivatized samples were analyzed by GC-MS using a DB-35MS column (30 m \times 0.25 mm i.d. \times 0.25 μm , Agilent J&W Scientific) installed in an Agilent 7890A gas chromatograph (GC) interfaced with an Agilent 5975C mass spectrometer (MS). Mass isotopomer distributions were determined by integrating metabolite ion fragments (Table S1) and corrected for natural abundance using in-house algorithms adapted from Fernandez et al. (1996).

Extraction of NAD^+ , NADH, NADP^+ , and NADPH and Analysis by LC-MS/MS

The extraction protocol for NADPH was based on one previously described by Fendt et al. (2013) and was optimized for analysis by LC-MS/MS. Briefly, cells were cultured in 6-well plates over the course of 30 min, washed once in ice-cold water, and immediately quenched in liquid nitrogen. A total of 200 μl ice-cold extraction buffer (40:40:20 acetonitrile/methanol/200 mM NaCl, 10 mM Tris-HCl [pH 9.2]) was added directly to the cells. Cells were scraped on ice and cleared by centrifugation at 4°C. A total of 50 μl of supernatant was transferred to a polypropylene vial, and samples were analyzed using a Q Exactive Benchtop LC-MS/MS (Thermo Fisher Scientific).

For measurement of NAD(P)H at 24 hr, cells were cultured in 10 cm plates. After 24 hr incubation with tracer, approximately 1×10^7 cells were washed in ice-cold 0.9% saline and immediately quenched in 1 ml of 80% methanol at -80°C . Cells were scraped on dry ice and cleared by centrifugation at 4°C. Cleared supernatant was transferred to Eppendorf tube, dried under vacuum using a CentriVap (Labconco), resuspended in water, and immediately loaded onto a XSELECT HSS XP 150 mm \times 2.1 mm \times 2.5 μm (Waters, Milford,

MA) with an UFLC XR HPLC (Shimadzu, Columbia, MD) coupled to an AB SCIEX Qtrap 5500 mass spectrometer (AB SCIEX, Framingham, MA) operating in negative ion mode. Mass isotopomer distributions were corrected for natural abundance using in-house software adapted from Fernandez et al. (1996). Additional information regarding chromatographic separation, mass spectrometry, and data acquisition can be found in the [Supplemental Experimental Procedures](#).

Isotopomer Spectral Analysis

The ISA method compares a measured palmitate mass isotopomer distribution to one that is simulated using a reaction network for palmitate synthesis whereby 14 NADPH molecules are consumed to form one palmitate molecule. Models were also generated for myristate and stearate synthesis whereby 12 or 16 NADPH molecules are consumed to form one myristate or stearate molecule, respectively. Parameters for the relative enrichment of the lipogenic NADPH pool from a given [²H] tracer and the percentage of fatty acids that are de novo synthesized are extracted from a best-fit model using the INCA MFA software package (Figure S2) (Young, 2014). The 95% confidence intervals for both parameters were estimated by evaluating the sensitivity of the sum of squared residuals between measured and simulated palmitate mass isotopomer distributions to small flux variations (Antoniewicz et al., 2006).

Cell Proliferation Assays

On day -1, 1/10 of a confluent 10 cm dish of cells was seeded in six 6-wells of a 6-well plate. Twenty-four hours later, cells were counted on an automated cell counter (Nexcelom), and this time point was considered T₀. At T₀, all other time points were media changed to ± doxycycline media (0.1 μg/mL doxycycline hyclate [Sigma] in water). Cells were counted every 24 hr in technical duplicate and biological triplicate. Media was changed every 48 hr to prevent degradation of doxycycline in the media.

SUPPLEMENTAL INFORMATION

Supplemental Information includes five figures, one table, and Supplemental Experimental Procedures and can be found with this article at <http://dx.doi.org/10.1016/j.molcel.2014.05.008>.

AUTHOR CONTRIBUTIONS

C.A.L. and S.J.P. conducted stable isotope-tracing experiments and prepared samples for GC-MS and LC-MS analysis. N.I.V. and C.R.G. conducted stable isotope tracing experiments and analyzed samples by GC-MS. C.R.G. assisted in serine- and glycine-tracing experiments for GC-MS analysis. C.A.L. and S.J.P. ran and analyzed samples on GC-MS. B.P.F., D.Y.G., D.M., and A.M.F. developed methods and ran samples on LC-MS. C.A.L. and S.J.P. analyzed data obtained by LC-MS (assisted by B.P.F. and D.M.). S.J.P. built the isotopomer spectral analysis method and carried out lipid modeling. C.A.L. generated inducible mutant IDH expression system. C.M.M., M.G.V.H., C.A.L., and S.J.P. designed the experiments. C.A.L., S.J.P., C.M.M., and M.G.V.H. designed the study, analyzed all data, and wrote the manuscript.

ACKNOWLEDGMENTS

We thank Michael Pacold, Elizaveta Freinkman, David Sabatini, and Bernhard Palsson for providing access to equipment. We are grateful to Patrick Ward and Craig B. Thompson for providing the cDNA for *IDH1-R132H* and *IDH2-R172K*. Eric L. Bell and Sarah-Maria Fendt provided advice and reagents. This work was supported in part by NIH grants P30CA147882, U54-CA121852-09, and R01CA168653, as well as by the Koch Institute/DFHC Bridge Project, the Koch Institute Frontier Research and Kathy and Curt Marble Cancer Research Fund, the Burroughs Wellcome Fund, the Damon Runyon Cancer Research Foundation, American Cancer Society grant IRG #70-002, DOD grant W81XWH-13-1-0105, a University of California Cancer Research Coordinating Committee grant, and a Searle Scholar Award.

Received: April 5, 2014
Revised: April 30, 2014
Accepted: May 6, 2014
Published: May 29, 2014

REFERENCES

- Ahler, E., Sullivan, W.J., Cass, A., Braas, D., York, A.G., Bensinger, S.J., Graeber, T.G., and Christofk, H.R. (2013). Doxycycline alters metabolism and proliferation of human cell lines. *PLoS ONE* 8, e64561.
- Anderson, D.D., Quintero, C.M., and Stover, P.J. (2011). Identification of a de novo thymidylate biosynthesis pathway in mammalian mitochondria. *Proc. Natl. Acad. Sci. USA* 108, 15163–15168.
- Antoniewicz, M.R., Kelleher, J.K., and Stephanopoulos, G. (2006). Determination of confidence intervals of metabolic fluxes estimated from stable isotope measurements. *Metab. Eng.* 8, 324–337.
- Bánhegyi, G., Csala, M., and Benedetti, A. (2009). Hexose-6-phosphate dehydrogenase: linking endocrinology and metabolism in the endoplasmic reticulum. *J. Mol. Endocrinol.* 42, 283–289.
- Barlowe, C.K., and Appling, D.R. (1988). In vitro evidence for the involvement of mitochondrial folate metabolism in the supply of cytoplasmic one-carbon units. *Biofactors* 1, 171–176.
- Ben-Yoseph, O., Kingsley, P.B., and Ross, B.D. (1994). Metabolic loss of deuterium from isotopically labeled glucose. *Magn. Reson. Med.* 32, 405–409.
- Bissell, M.J., Rambeck, W.A., White, R.C., and Bassham, J.A. (1976). Glycerol phosphate shuttle in virus-transformed cells in culture. *Science* 191, 856–858.
- Dang, L., White, D.W., Gross, S., Bennett, B.D., Bittinger, M.A., Driggers, E.M., Fantin, V.R., Jang, H.G., Jin, S., Keenan, M.C., et al. (2009). Cancer-associated IDH1 mutations produce 2-hydroxyglutarate. *Nature* 462, 739–744.
- Diehn, M., Cho, R.W., Lobo, N.A., Kalisky, T., Dorie, M.J., Kulp, A.N., Qian, D., Lam, J.S., Ailles, L.E., Wong, M., et al. (2009). Association of reactive oxygen species levels and radioresistance in cancer stem cells. *Nature* 458, 780–783.
- Fendt, S.M., Bell, E.L., Keibler, M.A., Olenchock, B.A., Mayers, J.R., Wasylenko, T.M., Vokes, N.I., Guarente, L., Vander Heiden, M.G., and Stephanopoulos, G. (2013). Reductive glutamine metabolism is a function of the α-ketoglutarate to citrate ratio in cells. *Nat. Commun.* 4, 2236.
- Fernandez, C.A., Des Rosiers, C., Previs, S.F., David, F., and Brunengraber, H. (1996). Correction of ¹³C mass isotopomer distributions for natural stable isotope abundance. *J. Mass Spectrom.* 31, 255–262.
- Go, M.K., Amyes, T.L., and Richard, J.P. (2009). Hydron transfer catalyzed by triosephosphate isomerase. Products of the direct and phosphite-activated isomerization of [1-¹³C]-glycolaldehyde in D(2)O. *Biochemistry* 48, 5769–5778.
- Grassian, A.R., Parker, S.J., Davidson, S.M., Divakruni, A.S., Green, C.R., Zhang, X., Slocam, K.L., Pu, M., Lin, F., Vickers, C., et al. (2014). IDH1 mutations alter citric acid cycle metabolism and increase dependence on oxidative mitochondrial metabolism. *Cancer Res.* Published online April 22, 2014. <http://dx.doi.org/10.1158/0008-5472.CAN-14-0772-T>.
- Hagedorn, C.H., and Phang, J.M. (1983). Transfer of reducing equivalents into mitochondria by the interconversions of proline and delta 1-pyrroline-5-carboxylate. *Arch. Biochem. Biophys.* 225, 95–101.
- Hellerstein, M.K., Greenblatt, D.J., and Munro, H.N. (1986). Glycoconjugates as noninvasive probes of intrahepatic metabolism: pathways of glucose entry into compartmentalized hepatic UDP-glucose pools during glycogen accumulation. *Proc. Natl. Acad. Sci. USA* 83, 7044–7048.
- Jain, M., Nilsson, R., Sharma, S., Madhusudhan, N., Kitami, T., Souza, A.L., Kafri, R., Kirschner, M.W., Clish, C.B., and Mootha, V.K. (2012). Metabolite profiling identifies a key role for glycine in rapid cancer cell proliferation. *Science* 336, 1040–1044.
- Jeon, S.M., Chandel, N.S., and Hay, N. (2012). AMPK regulates NADPH homeostasis to promote tumour cell survival during energy stress. *Nature* 485, 661–665.

- Jiang, P., Du, W., Mancuso, A., Wellen, K.E., and Yang, X. (2013). Reciprocal regulation of p53 and malic enzymes modulates metabolism and senescence. *Nature* 493, 689–693.
- Kardon, T., Senesi, S., Marcolongo, P., Legeza, B., Bánhegyi, G., Mandl, J., Fulceri, R., and Benedetti, A. (2008). Maintenance of luminal NADPH in the endoplasmic reticulum promotes the survival of human neutrophil granulocytes. *FEBS Lett.* 582, 1809–1815.
- Katz, J., and Rognstad, R. (1976). Futile cycles in the metabolism of glucose. *Curr. Top. Cell. Regul.* 10, 237–289.
- Katz, J., and Rognstad, R. (1978). Futile cycling in glucose-metabolism. *Trends Biochem. Sci.* 3, 171–174.
- Katz, J., Rognstad, R., and Kemp, R.G. (1965). Isotope discrimination effects in the metabolism of tritiated glucose. *J. Biol. Chem.* 240, PC1484–PC1486.
- Katz, J., Landau, B.R., and Bartsch, G.E. (1966). The pentose cycle, triose phosphate isomerization, and lipogenesis in rat adipose tissue. *J. Biol. Chem.* 241, 727–740.
- Kharroubi, A.T., Masterson, T.M., Aldaghas, T.A., Kennedy, K.A., and Kelleher, J.K. (1992). Isotopomer spectral analysis of triglyceride fatty acid synthesis in 3T3-L1 cells. *Am. J. Physiol.* 263, E667–E675.
- Kikuchi, G., Motokawa, Y., Yoshida, T., and Hiraga, K. (2008). Glycine cleavage system: reaction mechanism, physiological significance, and hyperglycemia. *Proc. Jpn. Acad., Ser. B, Phys. Biol. Sci.* 84, 246–263.
- LaNoue, K.F., and Schoolwerth, A.C. (1979). Metabolite transport in mitochondria. *Annu. Rev. Biochem.* 48, 871–922.
- LaNoue, K.F., Meijer, A.J., and Brouwer, A. (1974). Evidence for electrogenic aspartate transport in rat liver mitochondria. *Arch. Biochem. Biophys.* 161, 544–550.
- Levintow, L., and Eagle, H. (1961). Biochemistry of cultured mammalian cells. *Annu. Rev. Biochem.* 30, 605.
- Lunt, S.Y., and Vander Heiden, M.G. (2011). Aerobic glycolysis: meeting the metabolic requirements of cell proliferation. *Annu. Rev. Cell Dev. Biol.* 27, 441–464.
- Matsunaga, H., Futakuchi-Tsuchida, A., Takahashi, M., Ishikawa, T., Tsuji, M., and Ando, O. (2012). IDH1 and IDH2 have critical roles in 2-hydroxyglutarate production in D-2-hydroxyglutarate dehydrogenase depleted cells. *Biochem. Biophys. Res. Commun.* 423, 553–556.
- Metallo, C.M., and Vander Heiden, M.G. (2013). Understanding metabolic regulation and its influence on cell physiology. *Mol. Cell* 49, 388–398.
- Metallo, C.M., Gameiro, P.A., Bell, E.L., Mattaini, K.R., Yang, J., Hiller, K., Jewell, C.M., Johnson, Z.R., Irvine, D.J., Guarente, L., et al. (2012). Reductive glutamine metabolism by IDH1 mediates lipogenesis under hypoxia. *Nature* 481, 380–384.
- Nikiforov, A., Dölle, C., Niere, M., and Ziegler, M. (2011). Pathways and subcellular compartmentation of NAD biosynthesis in human cells: from entry of extracellular precursors to mitochondrial NAD generation. *J. Biol. Chem.* 286, 21767–21778.
- Nilsson, R., Jain, M., Madhusudhan, N., Sheppard, N.G., Strittmatter, L., Kampf, C., Huang, J., Asplund, A., and Mootha, V.K. (2014). Metabolic enzyme expression highlights a key role for MTHFD2 and the mitochondrial folate pathway in cancer. *Nat. Commun.* 5, 3128.
- Perry, C., Yu, S., Chen, J., Matharu, K.S., and Stover, P.J. (2007). Effect of vitamin B6 availability on serine hydroxymethyltransferase in MCF-7 cells. *Arch. Biochem. Biophys.* 462, 21–27.
- Pollak, N., Dölle, C., and Ziegler, M. (2007a). The power to reduce: pyridine nucleotides—small molecules with a multitude of functions. *Biochem. J.* 402, 205–218.
- Pollak, N., Niere, M., and Ziegler, M. (2007b). NAD kinase levels control the NADPH concentration in human cells. *J. Biol. Chem.* 282, 33562–33571.
- Reindina, A.R., Hermes, J.D., and Cleland, W.W. (1984). Use of multiple isotope effects to study the mechanism of 6-phosphogluconate dehydrogenase. *Biochemistry* 23, 6257–6262.
- Rühl, M., Le Coq, D., Aymerich, S., and Sauer, U. (2012). ¹³C-flux analysis reveals NADPH-balancing transhydrogenation cycles in stationary phase of nitrogen-starving *Bacillus subtilis*. *J. Biol. Chem.* 287, 27959–27970.
- Sazanov, L.A., and Jackson, J.B. (1994). Proton-translocating transhydrogenase and NAD- and NADP-linked isocitrate dehydrogenases operate in a substrate cycle which contributes to fine regulation of the tricarboxylic acid cycle activity in mitochondria. *FEBS Lett.* 344, 109–116.
- Schafer, Z.T., Grassian, A.R., Song, L., Jiang, Z., Gerhart-Hines, Z., Irie, H.Y., Gao, S., Puigserver, P., and Brugge, J.S. (2009). Antioxidant and oncogene rescue of metabolic defects caused by loss of matrix attachment. *Nature* 461, 109–113.
- Scotti, M., Stella, L., Shearer, E.J., and Stover, P.J. (2013). Modeling cellular compartmentation in one-carbon metabolism. *Wiley Interdiscip. Rev. Syst. Biol. Med.* 5, 343–365.
- Shin, K.J., Wall, E.A., Zavzavadjian, J.R., Santat, L.A., Liu, J., Hwang, J.I., Rebres, R., Roach, T., Seaman, W., Simon, M.I., and Fraser, I.D. (2006). A single lentiviral vector platform for microRNA-based conditional RNA interference and coordinated transgene expression. *Proc. Natl. Acad. Sci. USA* 103, 13759–13764.
- Son, J., Lyssiotis, C.A., Ying, H., Wang, X., Hua, S., Ligorio, M., Perera, R.M., Ferrone, C.R., Mullarky, E., Shyh-Chang, N., et al. (2013). Glutamine supports pancreatic cancer growth through a KRAS-regulated metabolic pathway. *Nature* 496, 101–105.
- Szárás, P., Bánhegyi, G., and Benedetti, A. (2010). Altered redox state of luminal pyridine nucleotides facilitates the sensitivity towards oxidative injury and leads to endoplasmic reticulum stress dependent autophagy in HepG2 cells. *Int. J. Biochem. Cell Biol.* 42, 157–166.
- Tedeschi, P.M., Markert, E.K., Gounder, M., Lin, H., Dvorzhinski, D., Dolfi, S.C., Chan, L.L., Qiu, J., DiPaola, R.S., Hirshfield, K.M., et al. (2013). Contribution of serine, folate and glycine metabolism to the ATP, NADPH and purine requirements of cancer cells. *Cell Death Dis.* 4, e877.
- Tibbetts, A.S., and Appling, D.R. (2010). Compartmentalization of Mammalian folate-mediated one-carbon metabolism. *Annu. Rev. Nutr.* 30, 57–81.
- Vander Heiden, M.G., Chandel, N.S., Williamson, E.K., Schumacker, P.T., and Thompson, C.B. (1997). Bcl-xL regulates the membrane potential and volume homeostasis of mitochondria. *Cell* 91, 627–637.
- Ward, P.S., Patel, J., Wise, D.R., Abdel-Wahab, O., Bennett, B.D., Collier, H.A., Cross, J.R., Fantin, V.R., Hedvat, C.V., Perl, A.E., et al. (2010). The common feature of leukemia-associated IDH1 and IDH2 mutations is a neomorphic enzyme activity converting alpha-ketoglutarate to 2-hydroxyglutarate. *Cancer Cell* 17, 225–234.
- Ward, P.S., Lu, C., Cross, J.R., Abdel-Wahab, O., Levine, R.L., Schwartz, G.K., and Thompson, C.B. (2013). The potential for isocitrate dehydrogenase mutations to produce 2-hydroxyglutarate depends on allele specificity and subcellular compartmentalization. *J. Biol. Chem.* 288, 3804–3815.
- Wise, D.R., Ward, P.S., Shay, J.E., Cross, J.R., Gruber, J.J., Sachdeva, U.M., Platt, J.M., DeMatteo, R.G., Simon, M.C., and Thompson, C.B. (2011). Hypoxia promotes isocitrate dehydrogenase-dependent carboxylation of α -ketoglutarate to citrate to support cell growth and viability. *Proc. Natl. Acad. Sci. USA* 108, 19611–19616.
- You, K.S. (1985). Stereospecificity for nicotinamide nucleotides in enzymatic and chemical hydride transfer reactions. *CRC Crit. Rev. Biochem.* 17, 313–451.
- Young, J.D. (2014). INCA: a computational platform for isotopically non-stationary metabolic flux analysis. *Bioinformatics* 30, 1333–1335.

IDH1 Mutations Alter Citric Acid Cycle Metabolism and Increase Dependence on Oxidative Mitochondrial Metabolism

Alexandra R. Grassian¹, Seth J. Parker⁴, Shawn M. Davidson³, Ajit S. Divakaruni⁵, Courtney R. Green⁴, Xiamei Zhang¹, Kelly L. Slocum¹, Minying Pu¹, Fallon Lin¹, Chad Vickers¹, Carol Joud-Caldwell¹, Franklin Chung¹, Hong Yin¹, Erika D. Handy⁴, Christopher Straub¹, Joseph D. Growney¹, Matthew G. Vander Heiden^{2,3}, Anne N. Murphy⁵, Raymond Pagliarini¹, and Christian M. Metallo^{4,6}

Abstract

Oncogenic mutations in isocitrate dehydrogenase 1 and 2 (IDH1/2) occur in several types of cancer, but the metabolic consequences of these genetic changes are not fully understood. In this study, we performed ¹³C metabolic flux analysis on a panel of isogenic cell lines containing heterozygous IDH1/2 mutations. We observed that under hypoxic conditions, IDH1-mutant cells exhibited increased oxidative tricarboxylic acid metabolism along with decreased reductive glutamine metabolism, but not IDH2-mutant cells. However, selective inhibition of mutant IDH1 enzyme function could not reverse the defect in reductive carboxylation activity. Furthermore, this metabolic reprogramming increased the sensitivity of IDH1-mutant cells to hypoxia or electron transport chain inhibition *in vitro*. Lastly, IDH1-mutant cells also grew poorly as subcutaneous xenografts within a hypoxic *in vivo* microenvironment. Together, our results suggest therapeutic opportunities to exploit the metabolic vulnerabilities specific to IDH1 mutation. *Cancer Res*; 74(12); 1–15. ©2014 AACR.

Introduction

Mutations in the metabolic enzymes isocitrate dehydrogenase 1 and 2 (IDH1/2) have been identified in a variety of tumor types, including acute myelogenous leukemia (AML), gliomas, cholangiocarcinomas, and chondrosarcomas (1–9). These mutations are almost exclusively heterozygous point mutations that occur in specific residues within the catalytic pocket, and are suggestive of activating, oncogenic mutations. Although IDH mutants are no longer capable of efficiently carrying out the normal oxidative reaction [converting isocitrate and NADP⁺ to α -ketoglutarate (α KG), CO₂, and NADPH], IDH mutations result in a novel gain-of-function involving the reductive, NADPH-dependent conversion of α KG to (D)2-hydroxyglutarate (2-HG;

refs. 10, 11). 2-HG is not typically present at high levels in normal cells but accumulates considerably in cells with IDH1/2 mutations as well as in the tumors of patients with IDH1/2 mutations, and has thus been termed an "oncometabolite" (10–12).

Research into the oncogenic function of mutant IDH1/2 has focused in large part on the effects of 2-HG. Numerous reports have linked 2-HG accumulation to epigenetic changes, which are thought to contribute to alterations in cellular differentiation status (13–22). Additional mutant IDH phenotypes have also been reported, including changes in collagen maturation and hypoxia inducible factor-1 α (HIF1 α) stabilization (21, 23). These changes likely occur through inhibition of α KG-dependent dioxygenase activity by high levels of 2-HG. However, the diverse roles that α KG-dependent dioxygenases play in the cell and the numerous phenotypes associated with mutant IDH and 2-HG suggest that the phenotypes downstream of 2-HG induction could be cell type- or context-specific. We hypothesize that metabolic alterations induced by IDH mutations may also be present and might be a general phenotype that offers additional approaches to target these tumors. Previous work suggests that overexpression of mutant IDH alters the levels of several metabolites (24) and leads to increased sensitivity to glutaminase inhibitors (25). Studies by Leonardi and colleagues have indicated that the IDH1-mutant enzymes compromise the ability of this enzyme to catalyze the reductive carboxylation reaction (26). However, it is unclear how IDH mutations affect central carbon metabolism in the heterozygous cellular setting, and further exploration into how these metabolic differences could be therapeutically exploited is warranted. An important distinction between IDH1 and IDH2 is their localization in the cytosol/peroxisome and

Authors' Affiliations: ¹Novartis Institutes for Biomedical Research; ²Koch Institute for Cancer Research, ³Massachusetts Institute of Technology, Cambridge, Massachusetts; Departments of ⁴Bioengineering and ⁵Pharmacology; and ⁶Moore's Cancer Center, University of California, San Diego, La Jolla, California

Note: Supplementary data for this article are available at Cancer Research Online (<http://cancerres.aacrjournals.org/>).

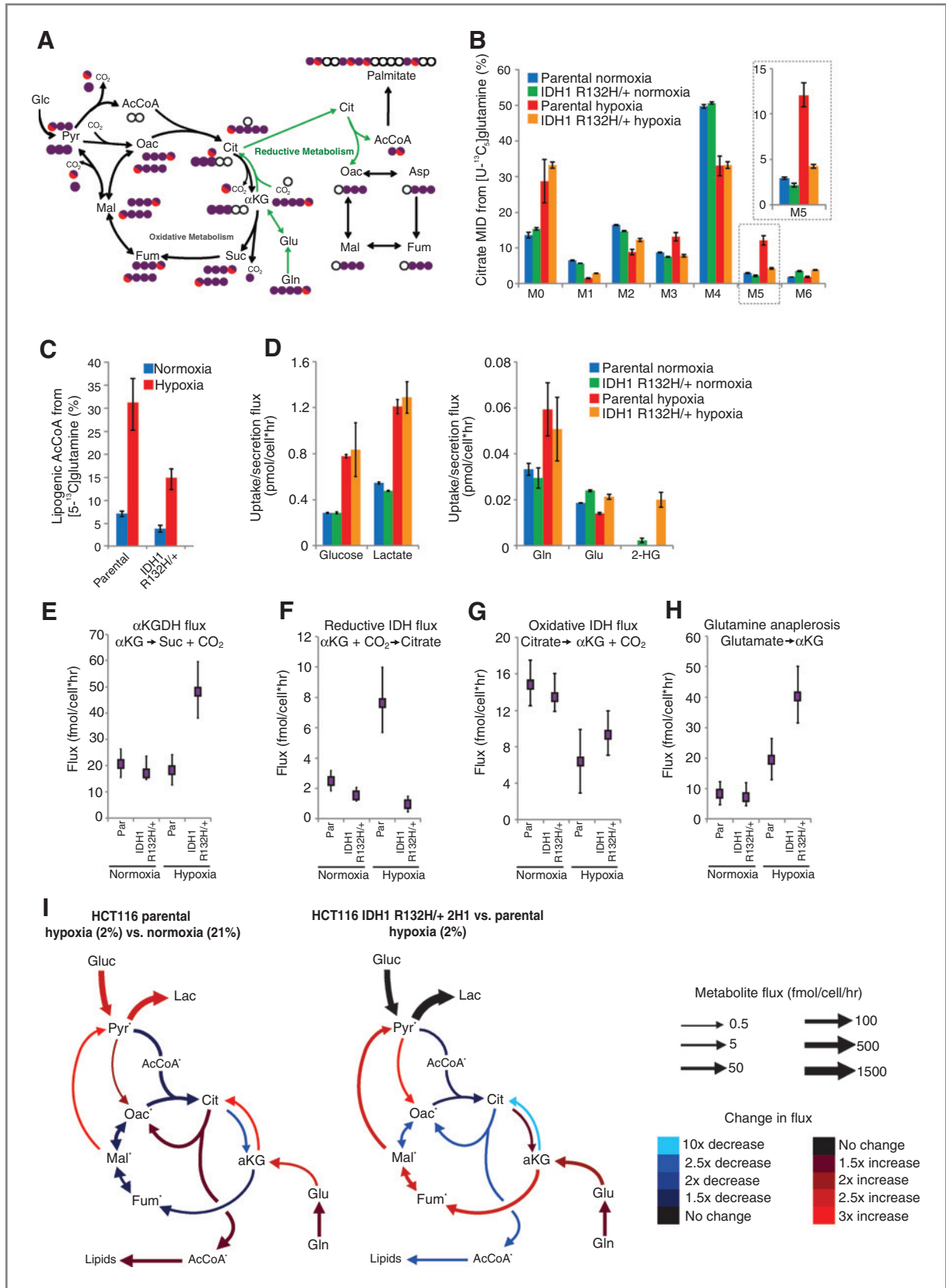
A.R. Grassian and S.J. Parker contributed equally to this work.

Current address of A.R. Grassian: Epizyme, Cambridge, MA.

Corresponding Authors: Christian M. Metallo, University of California, San Diego, 9500 Gilman Drive, MC-0412, La Jolla, CA 92093. Phone: 858-534-8209; Fax: 858-534-5722; E-mail: cmetallo@ucsd.edu; and Raymond Pagliarini, Novartis Institutes for Biomedical Research, 250 Massachusetts Avenue, Cambridge, MA 02139. Phone: 617-871-4307; E-mail: raymond.pagliarini@novartis.com

doi: 10.1158/0008-5472.CAN-14-0772-T

©2014 American Association for Cancer Research.



mitochondria, respectively, which may influence the ultimate metabolic phenotype of tumor cells with mutations in either enzyme.

Systems-based approaches that use stable isotope tracers (e.g., [¹³C]glutamine), mass spectrometry, and network modeling to estimate metabolic fluxes offer a unique means of characterizing intracellular metabolism (27). To understand the metabolic impact of heterozygous IDH mutation *in vitro*, we have applied ¹³C metabolic flux analysis (MFA) to a panel of cell lines that differ only with respect to their IDH1- and IDH2-mutant status. Using this approach, we have characterized how cells with wild-type (WT) and mutant IDH1/2 respond to hypoxia and pharmacologic induction of mitochondrial dysfunction.

Materials and Methods

Cell culture

HCT116 and MCF-10A isogenic clones were obtained from Horizon Discovery Ltd and IDH1/2 mutational status was verified by sequencing (28). HCT116 cells were cultured in McCoy's 5A Modified Medium with 10% FBS. D-2-HG treatments were done at 10 mmol/L and replenished every 48 hours. MCF-10A cells were cultured as described previously (28). HT-1080, SW1353, A549, and 143B cells were cultured in DMEM supplemented with 10% FBS. HT-1080 and SW1353 cells were obtained from the ATCC, and cells were tested and authenticated by single-nucleotide polymorphism fingerprinting. A549 cells were obtained from ATCC and were not further tested or authenticated. 143B cells were kindly provided by Dr. Leonard Guarente (Massachusetts Institute of Technology, Cambridge, MA) and were not further tested or authenticated. Cells were routinely cultured in normoxia (21% O₂) and then moved to hypoxia (1%–3% O₂, as indicated in the figure legends) for 48 to 72 hours where indicated. Generation of the p⁰ cells is described in the Supplementary Methods. Xenograft assays are described in Supplementary Methods.

Steady-state labeling of organic, amino, and fatty acids was accomplished by culturing subconfluent cells in triplicate in tracer medium for 72 hours in a 6-well plate. Labeling studies of HCT116, SW1353, HT1080, A549, and 143B cells were performed in glucose or glutamine-free DMEM containing 10% FBS and 17.5 mmol/L [1,2-¹³C₂]glucose, 4 mmol/L [U-¹³C₅]glutamine, or 4 mmol/L [5-¹³C]glutamine. For the HCT116 isogenic cells, the initial seeding density was 150,000 cells per well except for the IDH1 R132H/+ 2H1, IDH1 R132C/+ 2A9, and IDH1 R32C/+ 3A4, which were 250,000 cells per well. Labeling studies of the MCF-10A cells were done in glutamine-free DMEM containing 4 mmol/mg/L [U-¹³C₅]glutamine, 5% horse serum, 20 ng/mL

EGF, 10 μg/mL insulin, 0.5 μg/mL hydrocortisone, and 100 ng/mL cholera toxin. Gas chromatography mass spectrometry (GC-MS) analysis is described in Supplementary Methods.

MFA

¹³C MFA was conducted using INCA, a software package based on the EMU framework (<http://mfa.vueinnovations.com>; ref. 29). Intracellular concentrations of free metabolites and intra- and extracellular fluxes were assumed to be constant over the course of the tracing experiment. Fluxes through a metabolic network comprising of glycolysis, the pentose phosphate pathway, the TCA cycle, biomass synthesis, and fatty acid synthesis were estimated by minimizing the sum of squared residuals between experimental and simulated MIDs and extracellular fluxes using nonlinear least squares regression (30). The best global fit was found after estimating 100 times using random initial guesses for all fluxes in the network. A χ^2 statistical test was applied to assess the goodness-of-fit using α of 0.01. The 95% confidence intervals for all fluxes in the network were estimated by evaluating the sensitivity of the sum of squared residuals to flux variations (30). Isotopomer Spectral Analysis was performed as previously described (31). See Supplementary Methods for further details of MFA.

Reagents

The following reagents were used at the doses indicated and as described in the text/figure legends: [1,2-¹³C₂]glucose, [3-¹³C]glucose, [U-¹³C₅]glutamine, [1-¹³C]glutamine, and [5-¹³C]glutamine (all from Cambridge Isotope Laboratories); IDH-C277 (Xcessbio); HIF1 α antibody (610958, BD Biosciences). Synthesis of IDH1i A is described in Supplementary Methods.

Determination of oxygen consumption

HCT 116 cells were grown at either normoxia or hypoxia (3% O₂), and respiration was measured using an XF^e96 analyzer (Seahorse Bioscience). Cell growth and assays at 3% O₂ were conducted using the Coy Dual Hypoxic Chambers for Seahorse XF^e Analyzer (Coy Laboratory Products, Inc.) as described in Supplementary Methods.

Proliferation assays

To calculate doubling time, cells were trypsinized and viable cells were quantified on a ViCell (Beckman-Coulter). Doubling times are presented as the average of three or more independent experiments.

To generate longer-term growth curves, cells were plated at 3,000 cells per well in a 96-well plate in triplicate. Twenty-four

Figure 1. Isogenic IDH1 mutation compromises metabolic reprogramming under hypoxia. A, carbon atom (represented by circles) transitions and tracers used to detect changes in flux: [U-¹³C₅]glutamine (purple circles) or [5-¹³C]glutamine (circle with red). The fifth carbon is lost during oxidative TCA metabolism but is retained on citrate, AcCoA, and palmitate in the reductive pathway (green arrows). B, citrate MID labeling from [U-¹³C₅]glutamine from HCT116 parental and HCT116 IDH1 R132H/+ clone 2H1 cells cultured in normoxia or hypoxia (2% oxygen) for 72 hours. Data, representative of more than three independent experiments. Inset highlights changes in % M5 citrate. C, contribution of [5-¹³C]glutamine to lipogenic AcCoA from cells cultured as in Fig. 1B. D, uptake and secretion fluxes for cells cultured as in Fig. 1B. E–H, α -Ketoglutarate dehydrogenase (E), reductive IDH (F), oxidative IDH (G), and glutamine anaplerosis (H) flux estimates and 95% confidence intervals by the ¹³C MFA model. I, graphical representation of fluxes determined via MFA. Arrow thickness, level of flux in HCT116 cells cultured in hypoxia. Color, fold difference between hypoxic and normoxic parental HCT116 cells (left) or between hypoxic HCT116 IDH1 R132H/+ 2H1 cells and hypoxic HCT116 parental cells (right). *, metabolites that were modeled as existing in separate mitochondrial and cytosolic pools. aKG, α -Ketoglutarate; cit, citrate; fum, fumarate; gluc, glucose; glu, glutamate; gln, glutamine; lac, lactate; mal, malate; oac, oxaloacetate; pyr, pyruvate. See also Supplementary Methods, Supplementary Fig. S2, and Supplementary Tables S1–S4 for details of MFA model, results, and data.

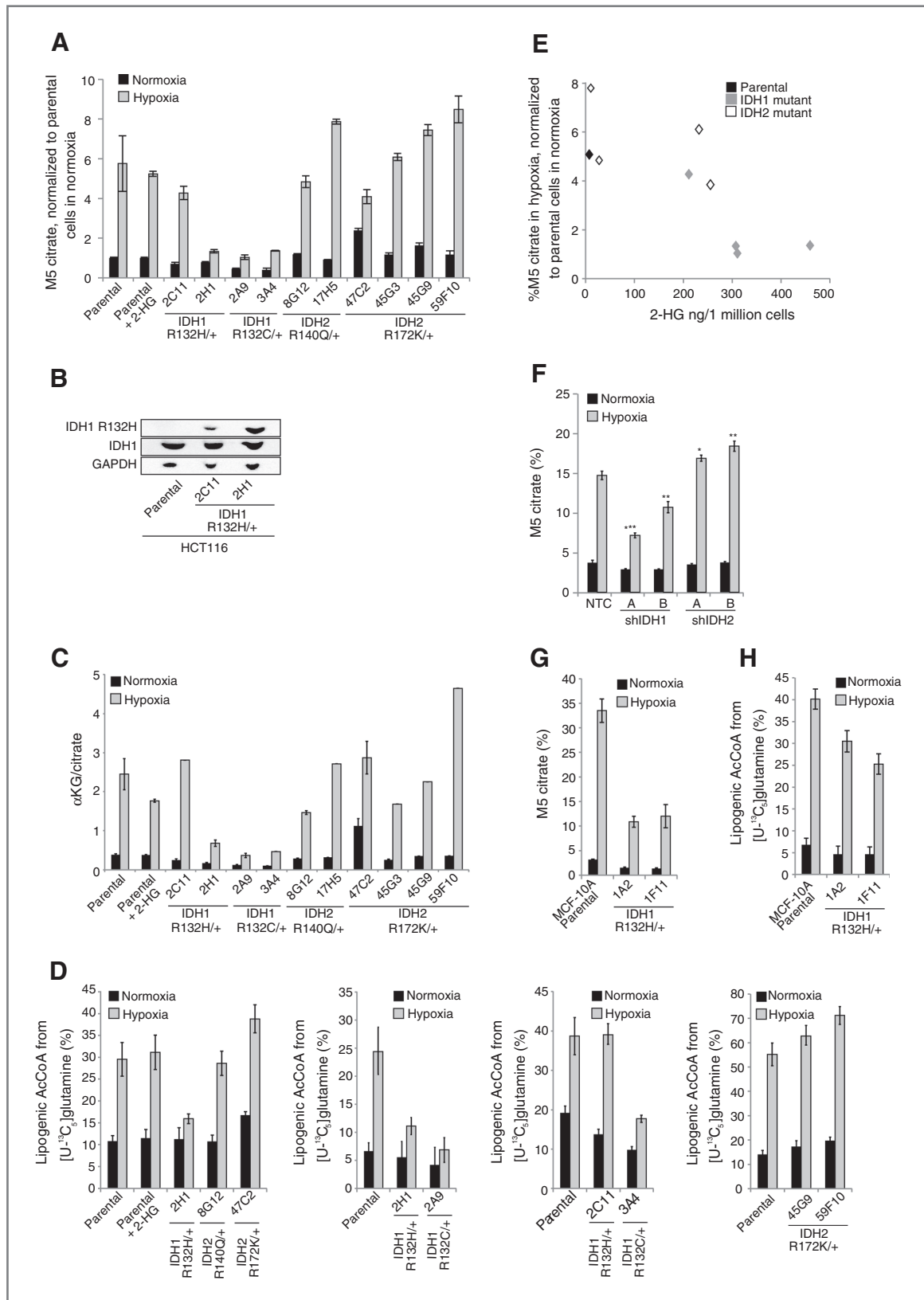


Figure 2. Compromised reductive TCA metabolism is specific to cells with mutant IDH1. A, relative level of reductive glutamine metabolism, determined by M5 labeling of citrate from [U-¹³C]₃glutamine in HCT116 parental cells with or without 10 mmol/L D-2-HG, or HCT116 IDH1/2-mutant isogenic cells cultured in normoxia or hypoxia (2% oxygen). Percentage of M5 citrate levels are normalized to HCT116 parental cells in normoxia for each experiment. (Continued on the following page.)

hours later, the indicated treatment was started and confluency measurements were taken every 12 hours for 108 to 216 hours using an Incucyte Kinetic Imaging System (Essen BioScience). Confluency data were modeled using a generalized logistic growth equation (equation 1), and the maximum growth rate was estimated using nonlinear regression:

$$Y = \frac{U - L}{1 + e^{-\mu_{\max}(t-t_0)}} + L \quad (1)$$

where U and L represent upper and lower asymptotes, t_0 represents the time at which cell confluency reaches 50%, and μ_{\max} represents the maximum growth rate per hour.

Pharmacologic profiling of the CCLE was performed as previously described (32). The growth inhibition assays are described in Supplementary Methods.

Statistical analysis

All results shown as averages of multiple independent experiments are presented as mean \pm SE; results shown as averages of technical replicates are presented as mean \pm SD. P values were calculated using a Student two-tailed t test; *, P value between 0.005 and 0.05; **, P value between 0.001 and 0.005; ***, P value $<$ 0.001. All errors associated with MFA and ISA of lipogenesis are 95% confidence intervals determined via sensitivity analysis.

Results

Mutant IDH1 compromises metabolic reprogramming under hypoxia

We and others have previously demonstrated that tricarboxylic acid (TCA) metabolism is reprogrammed under hypoxia, and flux through WT IDH1 and/or IDH2 become critical in these contexts (31, 33–37). Oncogenic mutations in IDH1 and IDH2 mitigate these enzymes' WT function and, in particular, the ability to catalyze the reductive carboxylation reaction while inducing a neomorphic activity that results in the accumulation of D-2-HG (11, 26). Therefore, we hypothesized that cancer cells harboring mutations in either IDH1 or IDH2 may be compromised in their ability to modulate metabolism under low oxygen tensions. To identify metabolic liabilities induced by IDH1 mutations, we applied ^{13}C MFA to isogenic HCT116 colon cancer cells with WT IDH1/2 (parental) or a heterozygous IDH1 mutation, IDH1 R132H/+ (clone 2H1). The IDH1-mutant, but not WT, cells have previously been shown to produce high levels of 2-HG (28). To gauge relative flux through the TCA cycle, each cell line was cultured in the presence of $[\text{U-}^{13}\text{C}_5]\text{glutamine}$ (uniformly ^{13}C -labeled glutamine) under normoxic or hypoxic (2% oxygen) conditions for

72 hours, and isotope enrichment in various metabolites was determined via mass spectrometry (Fig. 1A). Both cell lines displayed decreased oxidative TCA flux (as evidenced by decreased M3 αKG) in hypoxia (Supplementary Fig. S1A). Although minimal changes in labeling were detected when comparing the mass isotopomer distribution (MID) of citrate in each cell type grown in normoxia (designated as M0, M1, M2, etc. mass isotopomers, corresponding to ion fragments containing zero, one, or two ^{13}C , respectively), more significant deviations occurred in cells proliferating under hypoxia (Fig. 1B). Parental cells under hypoxia exhibited increased M5 labeling indicative of reductive carboxylation (Fig. 1B), as has been seen previously for many WT IDH1/2 cell lines (31, 33, 35). In contrast, the IDH1 R132H/+ cells showed only a slight increase in the abundance of this mass isotopomer under hypoxia (Fig. 1B). M5 citrate can also be produced via M6 citrate and glutaminolysis (38); however, no increase in the low basal levels of M6 citrate was observed in hypoxia (Fig. 1B). We observed similar changes in the labeling of other TCA metabolites, including M3 fumarate, malate, and aspartate (derived from oxaloacetate), further supporting our finding that IDH1-mutant cells display compromised reductive glutamine metabolism in hypoxia (Fig. 1A and Supplementary Fig. S1B–S1D). To further quantify the metabolism of glutamine through the reductive carboxylation pathway in these cells, we determined the contribution of $[\text{5-}^{13}\text{C}]\text{glutamine}$ to palmitate synthesis using isotopomer spectral analysis (ISA), as this tracer specifically labels acetyl coenzyme A (AcCoA) through the reductive carboxylation pathway (Fig. 1A; ref. 39). Although parental cells increased the contribution of glutamine to lipogenic AcCoA almost 5-fold under hypoxia, cells with a mutant IDH1 allele were compromised in their ability to increase this reductive carboxylation flux (Fig. 1C).

To characterize the metabolic phenotype of HCT116 cells with WT or IDH1 R132H/+ in a more comprehensive and unbiased manner, we incorporated uptake/secretion fluxes and mass isotopomer data into a network of central carbon metabolism. This model included glycolysis, the pentose phosphate pathway (PPP), TCA metabolism, and various biosynthetic fluxes using $[\text{U-}^{13}\text{C}_5]\text{glutamine}$ and $[\text{1,2-}^{13}\text{C}_2]\text{glucose}$ (for the oxidative PPP bifurcation), as these tracers provide optimal flux resolution throughout central carbon metabolism (40). An elementary metabolite unit (EMU)-based algorithm was used to estimate fluxes and associated confidence intervals in the network (41, 30), and a detailed description of the model, assumptions, and the complete data set are included as Supplementary Material. As expected, glucose and lactate fluxes were significantly increased by hypoxia in both cell lines, and significant 2-HG secretion occurred only in IDH1

(Continued.) B, Western blot of HCT116 parental, HCT116 IDH1 R132H/+ clone 2C11, and HCT116 IDH1 R132H/+ clone 2H1 showing levels of IDH1 R132H and total levels of IDH1. C, ratio of α -ketoglutarate to citrate from cells cultured as in Fig. 2A. D, contribution of $[\text{U-}^{13}\text{C}_5]\text{glutamine}$ to lipogenic AcCoA from cells cultured as in Fig. 2A. Four independent experiments are shown. E, correlation of reductive glutamine metabolism in 2% oxygen (as measured by % M5 citrate from $[\text{U-}^{13}\text{C}_5]\text{glutamine}$) to 2-HG ng/1 million cells. Note that HCT116 IDH2 R172K/+ 45G9 and 59F10 are not included in this figure. F, relative level of reductive glutamine metabolism, determined by M5 labeling of citrate from $[\text{U-}^{13}\text{C}_5]\text{glutamine}$ in HCT116 parental cells, which were stably infected with doxycycline-inducible shRNA's targeting IDH1 or IDH2, or nontargeting control (NTC). Cells were cultured for 48 hours in normoxia or hypoxia (1% oxygen) in the presence of 100 ng/mL doxycycline. Citrate labeling was determined via liquid chromatography/mass spectrometry. G, relative level of reductive glutamine metabolism, determined by M5 labeling of citrate from $[\text{U-}^{13}\text{C}_5]\text{glutamine}$ in MCF-10A cells cultured in normoxia or hypoxia (2% oxygen) for 72 hours. H, contribution of $[\text{U-}^{13}\text{C}_5]\text{glutamine}$ to lipogenic AcCoA from cells cultured as in Fig. 2G.

R132H/+ cells (Fig. 1D). Notably, 2-HG secretion was elevated under hypoxia, consistent with previous observations of 2-HG accumulation at low oxygen tension (33).

The modeling data comparing parental HCT116 cells grown in normoxia and hypoxia highlight some of the important metabolic changes that occur at low oxygen tensions (Fig. 1E–I, Supplementary Fig. S2, and Supplementary Tables S1–S4). In the HCT116 parental cells, pyruvate dehydrogenase and oxidative TCA metabolism are decreased under hypoxia, whereas pyruvate cycling through malic enzyme (ME) and pyruvate carboxylase (PC) are elevated under these conditions. Parental cells increased reductive IDH flux several fold, such that net IDH flux slightly favored the direction of reductive carboxylation (Fig. 1F, G, and I). As with the MID changes (Fig. 1B), only modest changes in metabolism were detected when comparing parental HCT116 cells with IDH1 R132H/+ 2H1 grown under normoxia (Fig. 1E–H and Supplementary Tables S1–S4). However, mutant cells maintained high oxidative IDH and α KG-dehydrogenase (α KGDH) fluxes and were unable to induce reductive carboxylation under hypoxia relative to the parental cells (Fig. 1E–G, I, and Supplementary Tables S1–S4). This oxidative TCA flux was maintained by increased glutamine anaplerosis and flux through ME and PC (Fig. 1H and I and Supplementary Tables S1–S4). Overall, these results demonstrate that significant reprogramming of TCA metabolism occurs in cells at 2% oxygen, and expression of IDH1 R132H/+ abrogates the cells' ability to respond appropriately to hypoxic stress.

Compromised reductive TCA metabolism is specific to cells with mutant IDH1

The MFA results above suggest that heterozygous IDH1 mutations disrupt the metabolic response of cells to hypoxic stress. To determine whether this metabolic deficiency is common to cells with either IDH1 or IDH2 mutations, we interrogated a panel of previously reported IDH1- and IDH2-mutant isogenic cells (28) and measured the ability of each to initiate reductive carboxylation under 2% oxygen. With the exception of IDH2 R140Q/+ cells, these mutant cell lines exhibit a ≥ 25 -fold increase in 2-HG compared with parental HCT116 cells (28). We cultured each clone with [U-¹³C₅]glutamine under normoxia and hypoxia, quantifying M5 citrate abundance (see Fig. 1A) to determine the relative extent of reductive carboxylation induction. All but one of the IDH1-mutant clones were consistently compromised in their ability to increase reductive carboxylation activity under hypoxia (Fig. 2A). The one exception being the IDH1 R132H/+ 2C11 clone, which showed a weaker phenotype relative to the other IDH1-mutant clones (Fig. 2A). This is likely explained by a lower level of IDH1 R132H protein (Fig. 2B) and lower level of 2-HG than the IDH1 R132H/+ 2H1 clone (28).

Unlike mutant IDH1 cells, HCT116 cells with IDH2 mutations exhibited levels of M5 citrate under hypoxia that were comparable with the parental cells (Fig. 2A). Addition of 10 mmol/L D-2-HG to the culture media also had a minimal effect on TCA metabolism (Fig. 2A). These data suggest that high 2-HG levels alone are unable to inhibit reductive carboxylation activity, even though this dose of exogenous D-2-HG is suffi-

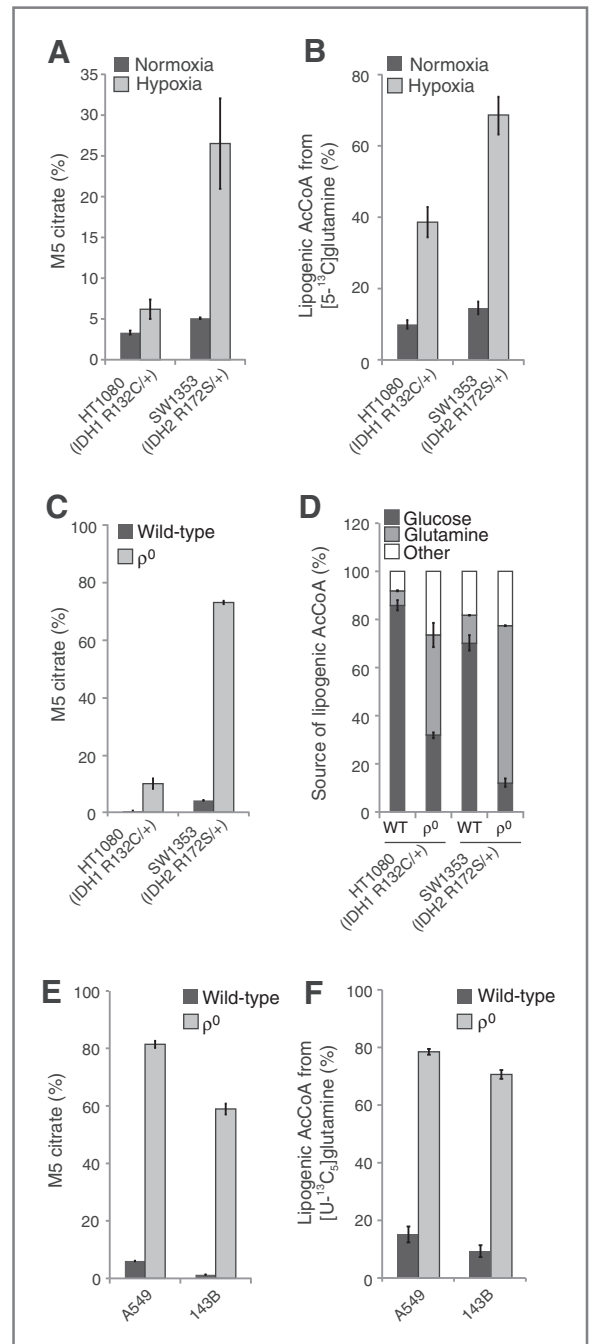
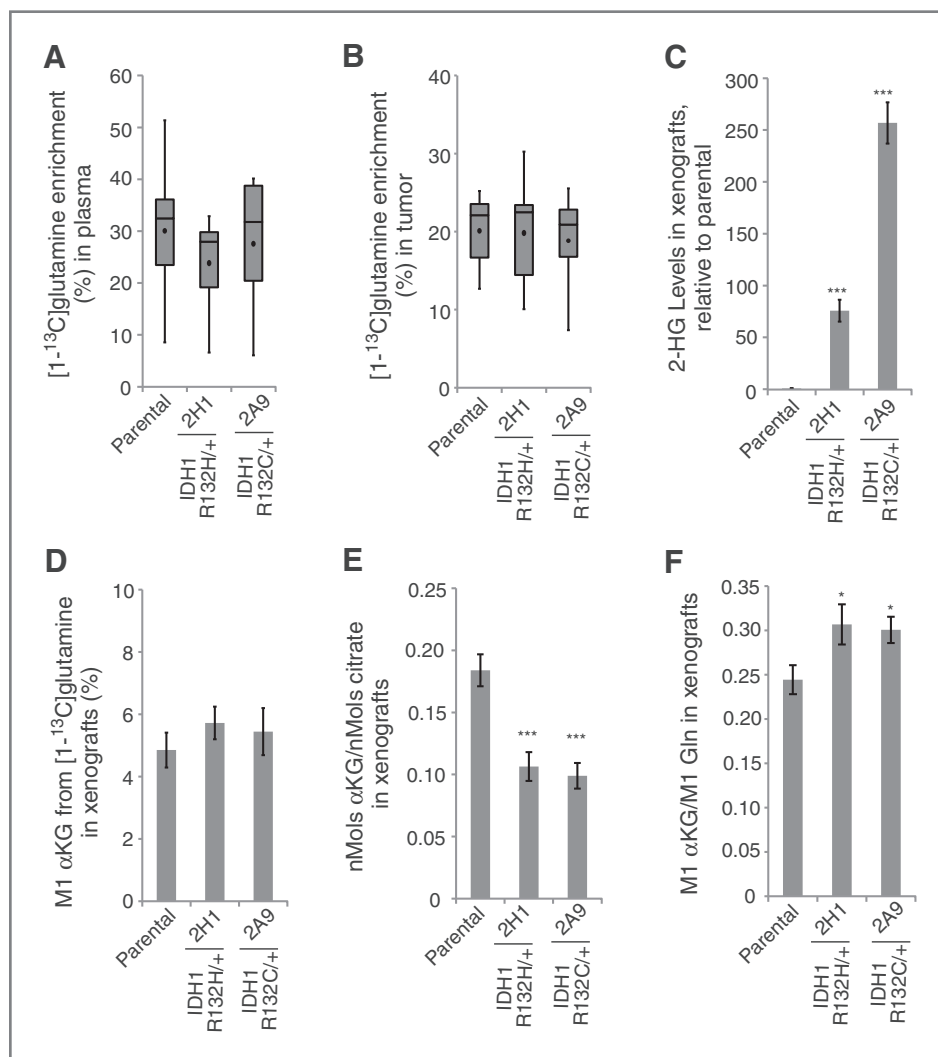


Figure 3. Cells with endogenous IDH1 and IDH2 mutations respond differently to mitochondrial stress. A, relative level of reductive glutamine metabolism, determined by M5 labeling of citrate from [U-¹³C₅]glutamine in HT-1080 and SW1353 cells cultured in normoxia or hypoxia (2% oxygen) for 72 hours. B, contribution of [5-¹³C]glutamine to lipogenic AcCoA from HT-1080 and SW1353 cells cultured in normoxia or hypoxia (1% oxygen) for 72 hours. C, relative level of reductive glutamine metabolism, determined by M5 labeling of citrate from [U-¹³C₅]glutamine in HT-1080 and SW1353 WT or p⁰ cells. D, contribution of [U-¹³C₅]glutamine and [U-¹³C₆]glucose to lipogenic AcCoA from cells cultured as in Fig. 3C. E, relative level of reductive glutamine metabolism, determined by M5 labeling of citrate from [U-¹³C₅]glutamine in A549 and 143B WT or p⁰ cells. F, contribution of [U-¹³C₅]glutamine to lipogenic AcCoA from cells cultured as in Fig. 3E.

Figure 4. Mutant IDH1 affects TCA metabolism *in vivo*. A and B, box-whisker plots showing [^{13}C]glutamine enrichment in plasma (A) and tumor (B) from mice with xenografts derived from the indicated cell lines. Black dot, mean; center line, median; box, interquartile range; whiskers, maximum and minimum values. C, relative 2-HG levels from xenografts, normalized to HCT116 parental xenografts. D, percentage of M1 αKG derived from [^{13}C]glutamine in tumor xenografts. E, nMols αKG /nMols citrate ratio from xenografts grown from the indicated HCT116 cells. F, glutamine anaplerosis, as determined by M1 labeling of αKG relative to M1 labeling of glutamine from xenografts grown from the indicated HCT116 cells.



cient to induce the 2-HG-dependent epithelial-mesenchymal transition (EMT) phenotype previously described in these cell lines (28). Consistent changes were observed when normalizing M5 citrate to M5 glutamate (Supplementary Fig. S3A), and levels of M6 citrate were not high in any of the clones (Supplementary Fig. S3B), providing evidence that such changes are specific to the IDH/aconitase node of metabolism. Similar trends were also observed when measuring the ratio of αKG /citrate under normoxia and hypoxia (Fig. 2C), another metric that describes the extent of reductive versus oxidative IDH flux (36, 42). Finally, the contribution of glutamine to lipogenic AcCoA under hypoxia was significantly lower in cells with IDH1 mutations but not those with IDH2 mutations or exogenous 2-HG (Fig. 2D). Overall, the extent that each IDH1-mutant cell line produced 2-HG correlated with their ability to activate reductive carboxylation flux under hypoxia (Fig. 2E), whereas IDH2-mutant cells did not adhere to this trend.

We next conducted shRNA-mediated knockdown of IDH1 and IDH2 in parental HCT116 cells to examine the roles of WT

IDH1 and IDH2 in mediating reductive glutamine metabolism (Supplementary Fig. S3C and S3D). Knockdown of IDH1 decreased levels of M5 citrate in cell populations cultured with [$^{13}\text{C}_5$]glutamine, whereas cells expressing shRNAs targeting IDH2 exhibited the same or higher M5 citrate (Fig. 2F). These results are consistent with previous studies in other cell lines (31), highlighting the importance of WT IDH1 expression in reprogramming TCA metabolism under hypoxia, and further suggest that IDH1 mutation selectively impedes WT IDH1 function in these cells.

To determine whether this mutant IDH1-induced metabolic deficiency is specific to the HCT116 genetic background or more broadly applicable to cells of different tissue origin, we performed similar analyses using MCF-10A immortalized mammary epithelial cells with heterozygous IDH1 mutations (28). When cultured for 3 days under normoxia or hypoxia, two distinct IDH1 R132H/+ clones were compromised in their ability to generate M5 citrate or lipogenic AcCoA from [$^{13}\text{C}_5$]glutamine (Fig. 2G and H and Supplementary Fig. S3E). Thus, cells with heterozygous IDH1 mutations, but not

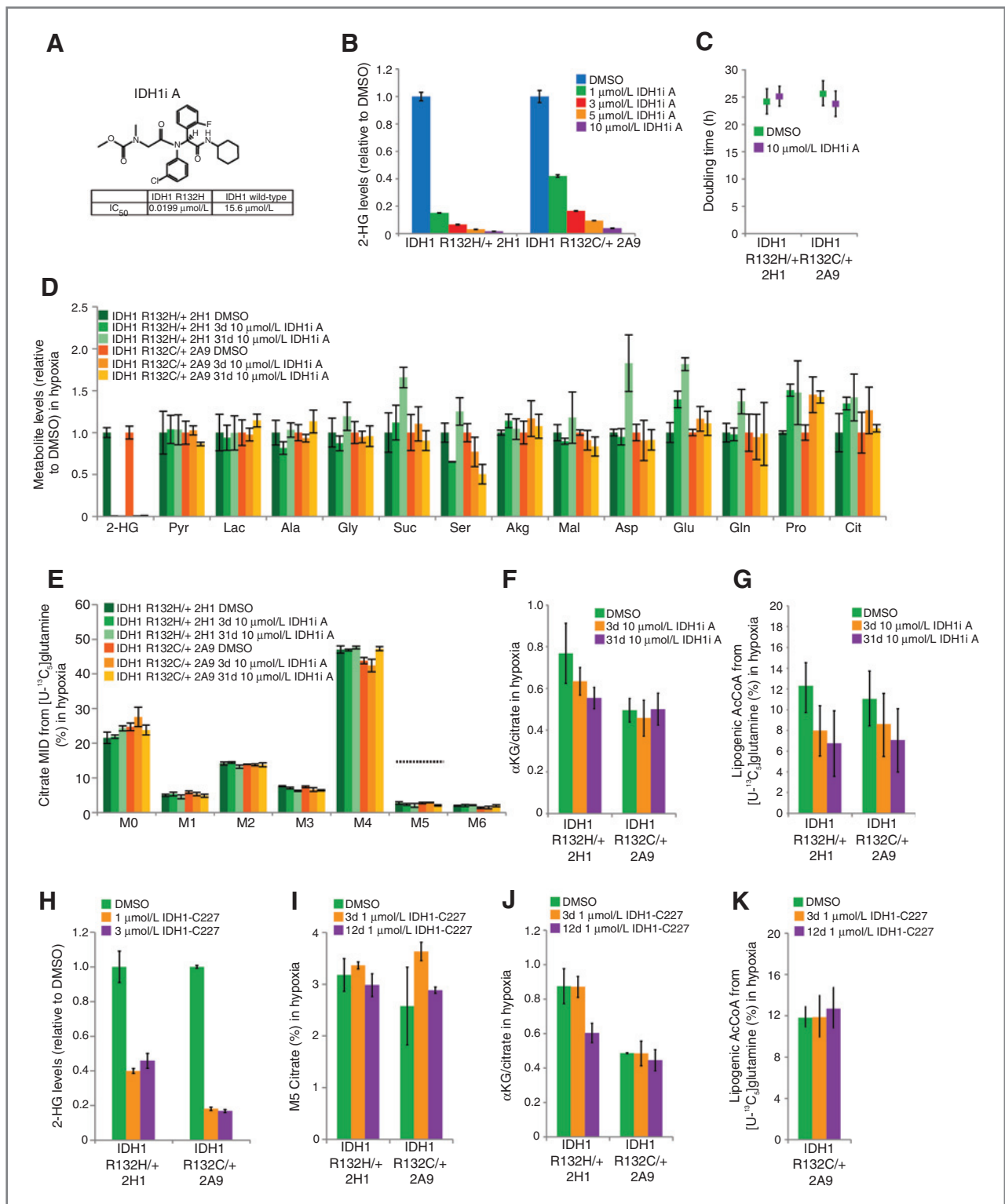


Figure 5. Inhibition of mutant IDH1 does not rescue reprogramming of TCA metabolism. **A**, structure and biochemical data for mutant IDH1 inhibitor, IDH1i A. Note that this is the (S) enantiomer. **B**, 2-HG levels in HCT116 IDH1 R132H/+ 2H1 and HCT116 IDH1 R132C/+ 2A9 cell lines treated with the indicated concentrations of IDH1i A for 3 days. **C**, doubling time of cells cultured with or without 10 μmol/L of IDH1i A. **D**, change in total metabolite levels of HCT116 IDH1 R132H/+ 2H1 and HCT116 IDH1 R132C/+ 2A9 cells cultured in the presence or absence of 10 μmol/L of IDH1i A for 3 or 31 days, the final 72 hours of which the cells are grown in hypoxia (2% oxygen). **E**, citrate MID labeling from [U-¹³C₃]glutamine from cells cultured as in Fig. 5D. Dotted line over M5 citrate represents average % M5 citrate observed in HCT116 parental cells cultured in hypoxia. (Continued on the following page.)

IDH2 mutations or exogenous 2-HG, are compromised for glutamine reductive carboxylation under hypoxia.

Cells with endogenous IDH1 and IDH2 mutations respond differently to mitochondrial stress

To examine whether these trends are observed in cell lines from cancers with endogenous IDH mutations, we evaluated the ability of two cell lines harboring IDH1 or IDH2 mutations to activate reductive carboxylation under conditions of mitochondrial stress. When switched to hypoxic growth, HT1080 IDH1 R132C/+ fibrosarcoma cells exhibited a significantly decreased ability to induce reductive glutamine metabolism in comparison with SW1353 IDH2 R172S/+ chondrosarcoma cells (Fig. 3A and Supplementary Fig. S4A). HT-1080 cells also used less glutamine for *de novo* lipogenesis than the SW1353 cells in 1% oxygen tension (Fig. 3B). Thus, a cell line with an endogenous mutation in IDH1, but not IDH2, displays compromised reductive glutamine metabolism in hypoxia.

In addition to low oxygen tensions, an alternative means of inducing reductive TCA metabolism is through the inhibition of oxidative phosphorylation (OXPHOS; refs. 34, 42). To compromise OXPHOS, we generated ρ^0 cells that lack a functional electron transport chain (ETC) from various cell lines using established methods (43). As expected, oxidative mitochondrial metabolism was virtually extinguished, as evidenced by M3 and M3/M5 labeling of α KG in ρ^0 cells generated from IDH-mutant cells (HT1080 and SW1353) or other cancer cell lines with WT IDH1/2 (143B osteosarcoma, A549 non-small cell lung cancer; Supplementary Fig. S4B–S4E). However, HT1080 IDH1 R132C/+ ρ^0 cells were compromised in their ability to generate citrate and palmitate through reductive glutamine metabolism, whereas SW1353 and both of the IDH1/2 WT ρ^0 cell lines were able to efficiently induce reductive carboxylation and use glutamine for lipid synthesis (Fig. 3C–F). Both the HT1080 and SW1353 ρ^0 cells continued to use glucose for lipid synthesis, and this contribution was higher in the HT1080 ρ^0 cells (Fig. 3D). The increased glucose utilization in HT1080 ρ^0 cells compared with SW1353 ρ^0 cells was facilitated by anaplerosis through pyruvate carboxylase, as demonstrated by increased labeling in TCA intermediates from [3- 13 C]glucose (Supplementary Fig. S4F and S4G). These results provide evidence that hypoxia and mitochondrial dysfunction drive reprogramming of the TCA cycle, and cells with spontaneously acquired IDH1 mutations are unable to efficiently reprogram metabolism to induce reductive glutamine carboxylation.

Mutant IDH1 affects TCA metabolism *in vivo*

The metabolic deficiencies of IDH1-mutant cells occur at oxygen tensions that are likely to occur in solid tumors and some normal tissues (44). To determine whether these

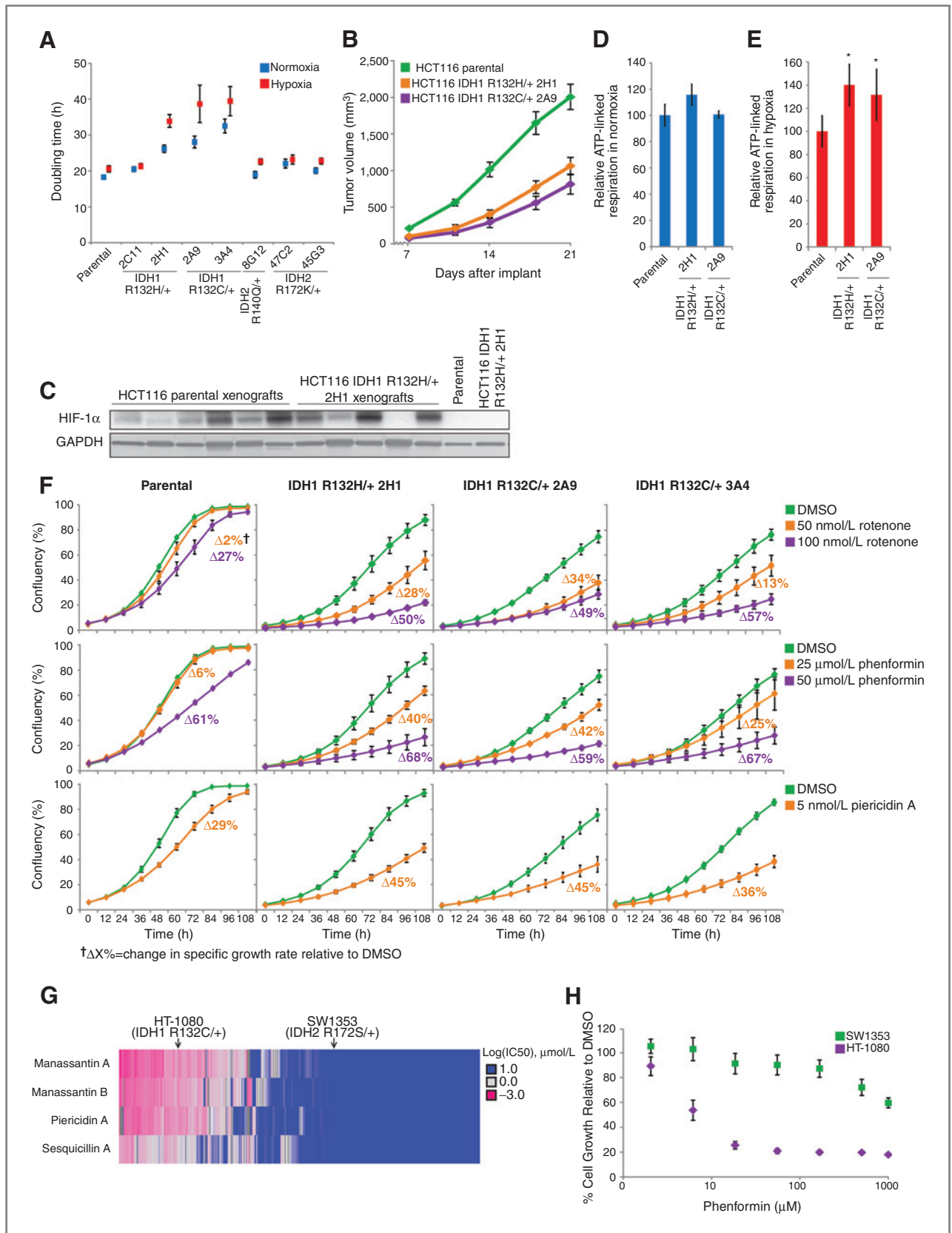
metabolic phenotypes arise *in vivo*, we generated subcutaneous xenografts using parental, IDH1 R132H/+ 2H1, and IDH1 R132C/+ 2A9 HCT116 cells. After tumors achieved a minimum diameter of 0.8 cm, mice were infused with [1- 13 C]glutamine for 6 hours to achieve steady-state isotope enrichment in plasma and tumor (Fig. 4A and B; ref. 45). A targeted metabolomic analysis was performed on plasma and tumor extracts to quantify isotope enrichment and metabolite abundances. Significant 2-HG was detected only in the IDH1-mutant tumors (Fig. 4C). Insufficient isotope enrichment was achieved in plasma and intratumoral glutamine/ α KG to detect label on citrate via reductive carboxylation (Fig. 4A, B, and D). However, in agreement with the results obtained from *in vitro* studies, the α KG/citrate ratio was significantly lower in IDH1-mutant tumors compared with those generated using parental HCT116 cells (Fig. 4E), indicating that TCA metabolism may also be perturbed in tumors comprised of IDH1-mutant cells. In addition, the contribution of glutamine anaplerosis to the α KG pool was significantly elevated in IDH1 R132H/+ and IDH1 R132C/+ tumors (Fig. 4F), which was also observed in our MFA results (Fig. 1H and I). Thus, the available data are consistent with our *in vitro* MFA results and provide evidence that TCA metabolism is similarly compromised by IDH1 mutations *in vivo*.

Inhibition of mutant IDH1 does not rescue reprogramming of TCA metabolism

One possible explanation for the decrease in reductive carboxylation flux in IDH1-mutant cells is that localized substrate (α KG and NADPH) consumption by the mutant enzyme for production of 2-HG compromises this activity. Therefore, we examined whether pharmacologic inhibition of mutant IDH1 could increase reductive carboxylation activity and rescue the ability of cells to use this pathway for growth under hypoxia. To test this hypothesis, we treated IDH1 R132H/+ 2H1 or IDH1 R132C/+ 2A9 cells with a mutant IDH1 inhibitor (IDH1i A) similar to a previously described structural class (Fig. 5A; refs. 22, 46). Doses of 10 μ mol/L were able to decrease 2-HG levels more than 25-fold in both clones (Fig. 5B). As would be expected from an engineered cell line that does not exhibit growth dependence on mutant IDH1 or 2-HG, 10 μ mol/L of IDH1i A had no appreciable effect on the growth rate of either cell line (Fig. 5C). Both short-term (3 day) and long-term (31 day) treatment with 10 μ mol/L IDH1i A induced minimal changes in metabolite abundances beyond 2-HG (Fig. 5D) and effectively reversed the mutant IDH-dependent EMT phenotype exhibited by these cells (Supplementary Fig. S5A).

IDH1i A did not rescue the ability of cells to initiate reductive TCA metabolism under hypoxia, as labeling of citrate (Fig. 5E) and other metabolites (Supplementary Fig. S5B–S5D) from

(Continued.) F, α KG/citrate ratio from cells cultured as in Fig. 5D. G, contribution of [U- 13 C₅]glutamine to lipogenic AcCoA from cells cultured as in Fig. 5D. H, 2-HG levels in HCT116 IDH1 R132H/+ 2H1 and HCT116 IDH1 R132C/+ 2A9 cell lines treated with the indicated concentration of IDH1-C227 for 3 days. I, relative level of reductive glutamine metabolism, determined by M5 labeling of citrate from [U- 13 C₅]glutamine in HCT116 IDH1 R132H/+ 2H1 and HCT116 IDH1 R132C/+ 2A9 cell lines treated with 1 μ mol/L of IDH1-C227 for 3 or 12 days, the final 72 hours of which the cells are grown in hypoxia (2% oxygen). J, α KG/citrate ratio from cells cultured as in Fig. 5I. K, contribution of [U- 13 C₅]glutamine to lipogenic AcCoA from cells cultured as in Fig. 5I.



[U-¹³C₅]glutamine was not increased compared with vehicle treatment. Other indices of reductive TCA metabolism, including the ratio of α KG/citrate and contribution of glutamine to lipid biosynthesis, also indicated that IDH1A failed to rescue reductive carboxylation flux in these cells (Fig. 5F and G). At 10 μ mol/L, the dose that showed maximal 2-HG inhibition, IDH1A mildly inhibited reductive carboxylation in the WT parental cells (Supplementary Fig. S5E and S5F), potentially due to off-target effects on WT IDH1 at high concentrations. To further address this issue, we also treated the IDH1-mutant cells with an additional inhibitor of mutant IDH1 at more moderate concentrations (Fig. 5H). We again observed no rescue in reductive glutamine metabolism (Fig. 5I–K), providing evidence that inhibition of IDH1-mutant activity may be insufficient to remove the block in metabolic reprogramming in response to hypoxic stress.

Cells expressing mutant IDH1 are sensitive to pharmacologic inhibition of mitochondrial oxidative metabolism

In comparing the growth rates of the HCT116 panel under normoxia and hypoxia, we observed that mutant IDH1 cells grew more poorly under conditions of low oxygen tension than parental cells or those expressing mutant IDH2 (Fig. 6A). HCT116 IDH1-mutant xenografts also grew at a significantly slower rate than the HCT116 parental cells (Fig. 6B), conditions that exhibited significant stabilization of HIF1 α in both parental and IDH1-mutant tumors (Fig. 6C). The growth rate of IDH2-mutant cells as xenografts was also significantly decreased relative to the parental cells (Supplementary Fig. S6A), though our available data do not yet support a hypothesis for how IDH2 mutations affect *in vivo* growth.

The slow growth of IDH1-mutant cells in the xenograft model suggests that altered TCA metabolism may contribute to the slower growth of these cells under the decreased oxygen levels *in vivo*. IDH1-mutant cells also exhibited increased oxidative TCA metabolism under hypoxia compared with parental cells (Fig. 1E and I), providing evidence that they are more dependent on OXPHOS. To further confirm this phenotype, we measured oxygen consumption in parental and IDH1-mutant cells under both normoxia and hypoxia. Consistent with our MFA results, basal respiration was not significantly altered in parental and IDH1-mutant cells under normoxic conditions, though uncoupled respiration was decreased in the IDH1-mutant cells (Supplementary Fig. S6B–S6E). Notably, mutant IDH1 cells exhibited significantly higher oligomycin-sensitive oxygen consumption under hypoxia compared with parental HCT116 cells, an

effect not reproduced under normoxia (Fig. 6D and E and Supplementary Fig. S6F and S6G). Therefore, we hypothesized that, as with growth in hypoxia, cells harboring IDH1 mutations may be more susceptible to inhibition of oxidative mitochondrial metabolism than cells with WT IDH1/2 or mutant IDH2.

To address this question, we cultured parental HCT116 cells and three IDH1-mutant clones in the presence of several compounds that inhibit Complex I of the ETC and OXPHOS. Confluency measurements were taken every 12 hours, and the maximum specific growth rate of each cell was determined using a generalized logistic growth model and compared with vehicle treatment for each cell line (Fig. 6F). The proliferation rate of cells with mutant IDH1 was significantly more affected than that of parental HCT116 cells in response to discrete dose ranges of Complex I inhibitors. On the other hand, the IDH2 R172K/+ cells displayed no such increased sensitivity with the same treatments (Supplementary Fig. S6H). This altered sensitivity is not due to differences in target modulation, as 100 nmol/L rotenone effectively shut down oxidative TCA cycle flux in all cells tested (Supplementary Fig. S6I). Treatment of parental HCT116 cells with 100 nmol/L rotenone also induced reductive carboxylation, whereas R132H/+ 2H1 and R132C/+ 2A9 HCT116 cells were less able to increase flux through this pathway (Supplementary Fig. S6J and S6K). Treatment with Antimycin A, an inhibitor of Complex III of the ETC, also inhibited oxidative TCA metabolism (Supplementary Fig. S6L). Induction of reductive carboxylation by Antimycin A was observed in the parental, but not IDH1-mutant, cells (Supplementary Fig. S6M and S6N). However, this compound had differential effects on succinate labeling compared with rotenone (Supplementary Fig. S6O). Notably, IDH1-mutant cells did not exhibit increased sensitivity to Antimycin A (Supplementary Fig. S6P), suggesting that Complex III inhibition suppresses growth through distinct mechanisms compared with Complex I inhibitors (e.g., reactive oxygen species generation, and pyrimidine synthesis; ref. 43). Thus, these data indicate that IDH1-, but not IDH2-, mutant cells are selectively sensitive to Complex I inhibitors.

To determine whether IDH1 mutants are generally more sensitive to other treatments, we examined the effect of the cell-cycle inhibitor flavopyridol in the HCT116 panel of cells. IDH1-mutant cells did not display increased sensitivity in comparison with parental or IDH2-mutant cells (Supplementary Fig. S6Q), further suggesting that the differential sensitivity we observe is specific to inhibitors of mitochondrial metabolism. These results indicate that oncogenic IDH1 mutations induce cells to rely more heavily on Complex I of the ETC, rendering these cancer cells more susceptible to inhibition of

Figure 6. Cells expressing mutant IDH1 are sensitive to pharmacologic inhibition of mitochondrial oxidative metabolism. A, doubling times of HCT116 cells cultured in normoxia or hypoxia (2% oxygen) for 72 hours. B, growth curves for HCT116 parental and IDH1-mutant xenografts. C, Western blot showing HIF1 α expression in HCT116 parental and HCT116 IDH1 R132H/+ 2H1 cells grown in normoxia in cell culture (last two lanes) or as xenografts. D, ATP-linked oxygen consumption for the indicated cell lines grown in normoxia. E, ATP-linked oxygen consumption for the indicated cell lines grown in hypoxia (3% O₂). F, growth charts from cells cultured as indicated. Images were acquired every 12 hours to measure confluency. Change in growth relative to DMSO treatment (Δ X%) was calculated using a generalized logistics growth model for batch culture and represents the change in the specific growth rate relative to the DMSO treatment for the indicated cell line. G, heatmap displaying IC₅₀ values to four inhibitors of mitochondrial metabolism for more than 500 cancer cell lines; HT-1080 and SW1353 cells are indicated. H, growth of HT-1080 and SW1353 cells under the indicated concentration of phenformin for 48 hours.

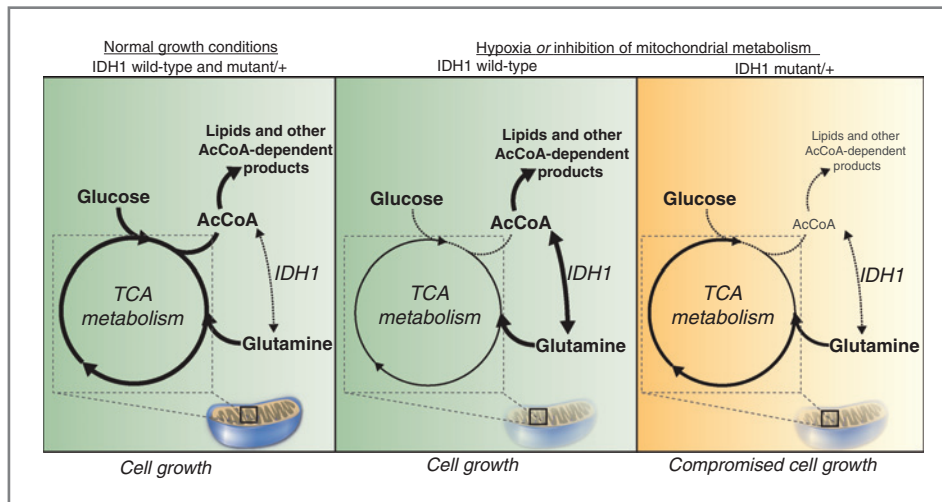


Figure 7. Mutant IDH1 sensitizes cells to inhibition of oxidative mitochondrial metabolism. Left, under normal growth conditions, glucose is metabolized oxidatively in the mitochondria, and AcCoA and lipids are derived mainly from glucose carbons. Middle, in IDH1 WT cells, inhibition of oxidative mitochondrial metabolism (induced by growth in hypoxia or pharmacologic inhibitors of the ETC) limits glucose flux to the mitochondria, and cells instead rely on reductive glutamine metabolism via IDH1 to provide carbons for AcCoA generation and lipid synthesis. Right, when oxidative mitochondrial metabolism is inhibited, cells with a mutant IDH1 allele are unable to fully induce reductive glutamine metabolism and are thus compromised for AcCoA and lipid production, leading to decreased cell growth.

this pathway compared with cells with WT IDH1/2 or mutant IDH2 alleles.

Finally, to evaluate whether these results are relevant to other cells, we interrogated the Cancer Cell Line Encyclopedia (CCLE; ref. 32), which contains compound sensitivity data across more than 500 cell lines for four ETC inhibitors (Fig. 6G; ref. 47). Cell lines clustered well into sensitive and insensitive groups, suggesting these compounds show consistent behavior across a wide panel of cell lines. Notably, IDH1-mutant HT1080 cells fell into the sensitive group, whereas IDH2-mutant SW1353 cells fell into the insensitive group (Fig. 6G). The differential effects of mitochondrial metabolism inhibitors were not likely due to HT1080 being generally more sensitive to compound treatments, as the sensitivities of HT1080 and SW1353 to a broad array of more than 1,300 compounds were within one SD of each other (Supplementary Fig. S6R). Furthermore, HT1080 cells were significantly more sensitive than SW1353 cells to phenformin treatment, a compound that was not included in the CCLE screening set (Fig. 6H). Together, these data indicate that IDH1 mutation may substantially sensitize cells to inducers of mitochondrial stress.

Discussion

Since the discovery of oncogenic mutations in IDH1 and IDH2, significant efforts have been made to elucidate the mechanisms driving tumorigenesis in these cancers. Owing to the accumulation of D-2-HG in these tumors, researchers have focused on the role of this oncometabolite in regulating the phenotype of IDH1/2-mutant cancer cells. For example, high D-2-HG levels and other metabolites regulate the activity of α KG-dependent dioxygenases that control many distinct cellular processes (12). However, the diverse roles of these enzymes in mediating activities ranging from collagen hydroxylation and HIF stabilization to epigenetics regulation com-

plicate identification of the specific process(es) driving tumorigenesis in each tumor type.

Despite the central role of these enzymes in cellular metabolism, surprisingly few investigations have addressed the metabolic changes that occur as a result of these genetic modifications. Here, we find that IDH1 mutations cause cells to increase flux through the oxidative TCA cycle, increase respiration, and compromise the conversion of glutamine to citrate, AcCoA, and fatty acids under hypoxia compared with those with WT IDH1 (Fig. 7). Others have previously shown that IDH1-mutant proteins are biochemically compromised with respect to this latter functionality, suggesting that cells harboring such mutations may be similarly defective under certain conditions (26). However, the cellular consequences of this effect have not been well characterized within intact, heterozygous, IDH-mutant cells. Proliferating cells must double their membrane lipids to successfully complete cell division, and evidence suggests that tumors may rely more on *de novo* lipogenesis than do nonneoplastic tissues, and inhibition of lipid synthesis decreases tumor growth *in vivo* (48, 49). In addition, AcCoA is an important precursor for a number of other molecules, including cholesterol, phospholipids, amino acid modifications, and histone acetylation (50). Interestingly, previous studies have also found that overexpression of mutant IDH leads to a decrease in N-acetyl amino acids, and these changes were also observed when comparing WT human glioma tissue with that of tumors with mutant IDH1 (24). This suggests that other AcCoA-dependent molecules may be similarly perturbed in the IDH1-mutant setting. Our application of MFA to IDH1-mutant cells builds upon these results by addressing the functional consequences of heterozygous IDH1 mutations and in particular the metabolic limitations that arise in tumors cells with these genetic modifications. Given the importance of each of these AcCoA-dependent processes for

cellular homeostasis and proliferation, we speculate that the reduced metabolic flexibility of these cells contributes to the decrease in growth rate that we observe in the IDH1-mutant cells under conditions of decreased oxidative mitochondrial metabolism.

Although 2-HG-mediated control of α KG-dependent dioxxygenase activity clearly plays a role in tumorigenesis driven by IDH mutations (13–18, 20–23), our results provide insights into therapeutic strategies that exploit the metabolic vulnerabilities caused by partial loss of WT IDH1 function. Interestingly, we observe that IDH1-mutant cells do not exhibit pronounced metabolic differences in normoxia; however, growth in low oxygen tensions or with pharmacologic inhibitors of mitochondrial metabolism results in the emergence of dramatic metabolic changes. Our MFA results identify several enzymes and pathways that are altered under hypoxia and in particular in the context of IDH1 mutations. Although compartment-specific IDH fluxes cannot be resolved with these data, these findings further highlight the importance of WT IDH1 activity in mediating reductive glutamine metabolism. Importantly, our results provide evidence that IDH1 mutations functionally compromise cellular metabolism under conditions of low oxygen levels, with the most pronounced effects being increased dependence on oxidative mitochondrial metabolism and an inability to induce reductive glutamine metabolism. We artificially induced such stresses using pharmacologic inhibitors of Complex I or manipulation of the oxygen tensions, and observed selective growth rate reductions in several IDH1-mutant cells, but not in parental or IDH2-mutant cancer cells. Other recent studies have also highlighted the importance of oxidative mitochondrial metabolism for tumor cell growth and survival both *in vitro* and *in vivo* (45, 51).

These results suggest that compromised IDH1 function may affect the proliferative capacity of tumor cells and furthermore that IDH1-mutant tumors may be sensitive to inhibitors that perturb mitochondrial metabolism. When comparing the metabolic phenotype of tumor xenografts derived from parental or IDH1-mutant cells with our *in vitro* results, similar changes were detected, including increased glutamine anaplerosis and a decreased α KG to citrate ratio. The increase in glutamine anaplerosis we observe in the IDH1-mutant cells is in agreement with previous findings, which suggest that IDH1-mutant cells display an increased sensitivity to glutaminase inhibitors (25). The similar metabolic changes that could be reliably measured *in vivo* suggest that the altered sensitivity we observe to inhibitors of mitochondrial metabolism *in vitro* may also be true *in vivo*. Additional studies are required to determine if cellular proliferation in the tumor microenvironment alone can drive hypoxia and induce reductive glutamine metabolism. Regardless, tumors would still be expected to increase their reliance on WT IDH1 (or cytosolic TCA) activity when treated with phenformin or other inhibitors of mitochondrial metabolism, suggesting that these strategies could be efficacious in IDH1-mutant cancers. As such, this increased susceptibility of cultured IDH1-mutant cells relative to parental cells or IDH2-mutant cells provides intriguing evidence of a potential therapeutic strategy associated with IDH1 mutational status and warrants further investigation in preclinical models.

We find that inhibition of mutant IDH1 is unable to reverse the observed metabolic phenotype. The DNA hypermethylator phenotype, which is highly associated with IDH mutation, is also not entirely reverted by a mutant IDH1 inhibitor (22), providing further evidence that some, but not all, mutant IDH-dependent phenotypes may be reversed by inhibitors targeting 2-HG production. Mechanistically, this result also suggests that the metabolic defect we observe may be independent of 2-HG production. A previous study used biochemical assays to quantify the effects of IDH1 mutations on reductive carboxylation activity, and, in agreement with our findings here, demonstrated that the mutant enzymes are unable to catalyze the conversion of α KG and CO_2 to isocitrate (26). This study concluded that the subunits in a WT/mutant heterodimer function independently; however, our modeling data indicate that heterozygous IDH1 mutations lead to a much greater than 50% inhibition of reductive glutamine metabolism (Fig. 1F), suggesting a possible dominant effect of the mutant protein in cells or alternatively global metabolic reprogramming in response to the compromised cytosolic IDH1 activity caused by these mutations.

Importantly, as small molecules capable of inhibiting mutant IDH1 enzymatic activity and preventing D-2-HG accumulation fail to rescue mutant cell metabolism under hypoxia, this suggests that combinatorial therapeutic strategies that block oncogenic D-2-HG production (e.g., via a mutant-selective inhibitor of enzyme function), while simultaneously targeting mutant IDH1-induced metabolic liabilities, may be a viable option for therapy. Such an approach could involve IDH1-mutant inhibitor treatment to attenuate any pro-survival or dedifferentiation effects of D-2-HG, while increasing the tumor's reliance on WT IDH1 activity through an inhibitor of oxidative mitochondrial metabolism. As drugs that could target the mutant IDH1 metabolic phenotype are already in the clinic (metformin, phenformin) and inhibitors of mutant IDH1 are currently being developed (22, 46), it is hoped that this hypothesis will be tested in the clinic in the near future.

Disclosure of Potential Conflicts of Interest

A.S. Divakaruni is a consultant/advisory board member of Seahorse Bioscience. M.G. Vander Heiden has ownership interest and is a consultant/advisory board member of Agios Pharmaceuticals. A.N. Murphy received a commercial research grant and is a consultant/advisory board member of Seahorse Bioscience. C. Straub, J.D. Growney, and R. Pagliarini have ownership interest in Novartis. C.M. Metallo has honoraria from the speakers' bureau of Agios Pharmaceuticals. No potential conflicts of interest were disclosed by the other authors.

Authors' Contributions

Conception and design: A.R. Grassian, S.J. Parker, X. Zhang, F. Lin, M.G. Vander Heiden, A.N. Murphy, R. Pagliarini, C.M. Metallo
Development of methodology: A.R. Grassian, S.J. Parker, S.M. Davidson, A.S. Divakaruni, X. Zhang, C. Vickers, C. Joud-Caldwell, F. Chung, H. Yin
Acquisition of data (provided animals, acquired and managed patients, provided facilities, etc.): A.R. Grassian, S.J. Parker, S.M. Davidson, A.S. Divakaruni, C.R. Green, X. Zhang, K.L. Slocum, M. Pu, F. Lin, F. Chung, H. Yin, E.D. Handy, C. Straub, J.D. Growney, A.N. Murphy, C.M. Metallo
Analysis and interpretation of data (e.g., statistical analysis, biostatistics, computational analysis): A.R. Grassian, S.J. Parker, S.M. Davidson, A.S. Divakaruni, C.R. Green, X. Zhang, M. Pu, F. Lin, C. Joud-Caldwell, H. Yin, J.D. Growney, A.N. Murphy, R. Pagliarini, C.M. Metallo

Writing, review, and/or revision of the manuscript: A.R. Grassian, S.J. Parker, S.M. Davidson, C.R. Green, X. Zhang, F. Lin, F. Chung, C. Straub, M.G. Vander Heiden, R. Pagliarini, C.M. Metallo

Administrative, technical, or material support (i.e., reporting or organizing data, constructing databases): A.R. Grassian, S.J. Parker, M. Pu, R. Pagliarini

Study supervision: A.R. Grassian, S.J. Parker, M.G. Vander Heiden, A.N. Murphy, R. Pagliarini, C.M. Metallo

Acknowledgments

The authors thank Nicholas Keen, William Sellers, Jonathan Coloff, Julian Levell, Charles Stiles, Juliet Williams, Brant Firestone, Wenlin Shao, Jonathan Solomon, Frank Stegmeier, and the Novartis Postdoctoral Fellows for helpful discussions of this work.

Grant Support

This work was supported by Novartis Institutes for Biomedical Research, American Cancer Society Institutional Research Grant 70-002 (C.M. Metallo),

the DOD Lung Cancer Research Program Grant W81XWH-13-1-0105 (C.M. Metallo), and a UC Cancer Research Coordinating Committee grant (C.M. Metallo). S.J. Parker is supported by the NIH/National Institute of Biomedical Imaging and Bioengineering Interfaces Training Grant. A.R. Grassian is the recipient of a presidential postdoctoral fellowship from Novartis Institutes for Biomedical Research. M.G. Vander Heiden and S.M. Davidson acknowledge support from NIH grants R01CA168653 and 5-P30-CA14051-39, and support from the Koch Institute/DFHCC Bridge Project, the Burrough's Wellcome Fund, the Smith Family, the Ludwig Foundation, and the Damon Runyon Cancer Research Foundation.

The costs of publication of this article were defrayed in part by the payment of page charges. This article must therefore be hereby marked advertisement in accordance with 18 U.S.C. Section 1734 solely to indicate this fact.

Received March 14, 2014; accepted March 21, 2014; published OnlineFirst April 22, 2014.

References

- Arai M, Nobusawa S, Ikota H, Takemura S, Nakazato Y. Frequent IDH1/2 mutations in intracranial chondrosarcoma: a possible diagnostic clue for its differentiation from chordoma. *Brain Tumor Pathol* 2012;29:201–6.
- Cairns RA, Iqbal J, Lemonnier F, Kucuc C, de Leval L, Jais JP, et al. IDH2 mutations are frequent in angioimmunoblastic T-cell lymphoma. *Blood* 2012;119:1901–3.
- Hayden JT, Fruhwald MC, Hasselblatt M, Ellison DW, Bailey S, Clifford SC. Frequent IDH1 mutations in supratentorial primitive neuroectodermal tumors (spNET) of adults but not children. *Cell Cycle* 2009;8:1806–7.
- Parsons DW, Jones S, Zhang X, Lin JC, Leary RJ, Angenendt P, et al. An integrated genomic analysis of human glioblastoma multiforme. *Science* 2008;321:1807–12.
- Yan H, Parsons DW, Jin G, McLendon R, Rasheed BA, Yuan W, et al. IDH1 and IDH2 mutations in gliomas. *N Engl J Med* 2009;360:765–73.
- Mardis ER, Ding L, Dooling DJ, Larson DE, McLellan MD, Chen K, et al. Recurring mutations found by sequencing an acute myeloid leukemia genome. *N Engl J Med* 2009;361:1058–66.
- Amary MF, Bacsi K, Maggiani F, Damato S, Halai D, Berisha F, et al. IDH1 and IDH2 mutations are frequent events in central chondrosarcoma and central and periosteal chondromas but not in other mesenchymal tumours. *J Pathol* 2011;224:334–43.
- Borger DR, Tanabe KK, Fan KC, Lopez HU, Fantin VR, Straley KS, et al. Frequent mutation of isocitrate dehydrogenase (IDH)1 and IDH2 in cholangiocarcinoma identified through broad-based tumor genotyping. *Oncologist* 2012;17:72–9.
- Wang P, Dong Q, Zhang C, Kuan PF, Liu Y, Jeck WR, et al. Mutations in isocitrate dehydrogenase 1 and 2 occur frequently in intrahepatic cholangiocarcinomas and share hypermethylation targets with glioblastomas. *Oncogene* 2012;1–10.
- Ward PS, Patel J, Wise DR, Abdel-Wahab O, Bennett BD, Collier HA, et al. The common feature of leukemia-associated IDH1 and IDH2 mutations is a neomorphic enzyme activity converting alpha-ketoglutarate to 2-hydroxyglutarate. *Cancer Cell* 2010;17:225–34.
- Dang L, White DW, Gross S, Bennett BD, Bittinger MA, Driggers EM, et al. Cancer-associated IDH1 mutations produce 2-hydroxyglutarate. *Nature* 2009;462:739–44.
- Yen KE, Schenkein DP. Cancer-associated isocitrate dehydrogenase mutations. *Oncologist* 2012;17:5–8.
- Xu W, Yang H, Liu Y, Yang Y, Wang P, Kim SH, et al. Oncometabolite 2-hydroxyglutarate is a competitive inhibitor of alpha-ketoglutarate-dependent dioxygenases. *Cancer Cell* 2011;19:17–30.
- Figuerola ME, Abdel-Wahab O, Lu C, Ward PS, Patel J, Shih A, et al. Leukemic IDH1 and IDH2 mutations result in a hypermethylation phenotype, disrupt TET2 function, and impair hematopoietic differentiation. *Cancer Cell* 2010;18:553–67.
- Lu C, Ward PS, Kapoor GS, Rohle D, Turcan S, Abdel-Wahab O, et al. IDH mutation impairs histone demethylation and results in a block to cell differentiation. *Nature* 2012;483:474–8.
- Turcan S, Rohle D, Goenka A, Walsh LA, Fang F, Yilmaz E, et al. IDH1 mutation is sufficient to establish the glioma hypermethylator phenotype. *Nature* 2012;483:479–83.
- Chowdhury R, Yeoh KK, Tian YM, Hillringhaus L, Bagg EA, Rose NR, et al. The oncometabolite 2-hydroxyglutarate inhibits histone lysine demethylases. *EMBO Rep* 2011;12:463–9.
- Sasaki M, Knobbe CB, Munger JC, Lind EF, Brenner D, Brustle A, et al. IDH1(R132H) mutation increases murine haematopoietic progenitors and alters epigenetics. *Nature* 2012;488:656–9.
- Wang F, Travins J, DeLaBarre B, Penard-Lacronique V, Schalm S, Hansen E, et al. Targeted inhibition of mutant IDH2 in leukemia cells induces cellular differentiation. *Science* 2013;340:622–6.
- Losman JA, Loofer RE, Koivunen P, Lee S, Schneider RK, McMahon C, et al. (R)-2-hydroxyglutarate is sufficient to promote leukemogenesis and its effects are reversible. *Science* 2013;339:1621–5.
- Koivunen P, Lee S, Duncan CG, Lopez G, Lu G, Ramkissoon S, et al. Transformation by the (R)-enantiomer of 2-hydroxyglutarate linked to EGLN activation. *Nature* 2012;483:484–8.
- Rohle D, Popovici-Muller J, Palaskas N, Turcan S, Grommes C, Campos C, et al. An inhibitor of mutant IDH1 delays growth and promotes differentiation of glioma cells. *Science* 2013;340:626–30.
- Sasaki M, Knobbe CB, Itsumi M, Elia AJ, Harris IS, Chio II, et al. D-2-hydroxyglutarate produced by mutant IDH1 perturbs collagen maturation and basement membrane function. *Genes Dev* 2012;26:2038–49.
- Reitman ZJ, Jin G, Karoly ED, Spasojevic I, Yang J, Kinzler KW, et al. Profiling the effects of isocitrate dehydrogenase 1 and 2 mutations on the cellular metabolome. *Proc Natl Acad Sci U S A* 2011;108:3270–5.
- Seltzer MJ, Bennett BD, Joshi AD, Gao P, Thomas AG, Ferraris DV, et al. Inhibition of glutaminase preferentially slows growth of glioma cells with mutant IDH1. *Cancer Res* 2010;70:8981–7.
- Leonardi R, Subramanian C, Jackowski S, Rock CO. Cancer-associated isocitrate dehydrogenase mutations inactivate NADPH-dependent reductive carboxylation. *J Biol Chem* 2012;287:14615–20.
- Zamboni N. ¹³C metabolic flux analysis in complex systems. *Curr Opin Biotechnol* 2011;22:103–8.
- Grassian AR, Lin F, Barrett R, Liu Y, Jiang W, Korpala M, et al. Isocitrate dehydrogenase (IDH) mutations promote a reversible ZEB1/microRNA (miR)-200-dependent epithelial-mesenchymal transition (EMT). *J Biol Chem* 2012;287:42180–94.
- Antoniewicz MR, Kelleher JK, Stephanopoulos G. Elementary metabolite units (EMU): a novel framework for modeling isotopic distributions. *Metab Eng* 2007;9:68–86.
- Antoniewicz MR, Kelleher JK, Stephanopoulos G. Determination of confidence intervals of metabolic fluxes estimated from stable isotope measurements. *Metab Eng* 2006;8:324–37.

31. Metallo CM, Gameiro PA, Bell EL, Mattaini KR, Yang J, Hiller K, et al. Reductive glutamine metabolism by IDH1 mediates lipogenesis under hypoxia. *Nature* 2012;481:380–4.
32. Barretina J, Caponigro G, Stransky N, Venkatesan K, Margolin AA, Kim S, et al. The Cancer Cell Line Encyclopedia enables predictive modelling of anticancer drug sensitivity. *Nature* 2012;483:603–7.
33. Wise DR, Ward PS, Shay JE, Cross JR, Gruber JJ, Sachdeva UM, et al. Hypoxia promotes isocitrate dehydrogenase-dependent carboxylation of alpha-ketoglutarate to citrate to support cell growth and viability. *Proc Natl Acad Sci U S A* 2011;108:19611–6.
34. Mullen AR, Wheaton WW, Jin ES, Chen PH, Sullivan LB, Cheng T, et al. Reductive carboxylation supports growth in tumour cells with defective mitochondria. *Nature* 2012;481:385–8.
35. Scott DA, Richardson AD, Filipp FV, Knutzen CA, Chiang GG, Ronai ZA, et al. Comparative metabolic flux profiling of melanoma cell lines: beyond the Warburg effect. *J Biol Chem* 2011;286:42626–34.
36. Fendt SM, Bell EL, Keibler MA, Olenchock BA, Mayers JR, Wasylenko TM, et al. Reductive glutamine metabolism is a function of the alpha-ketoglutarate to citrate ratio in cells. *Nat Commun* 2013;4:2236.
37. Gameiro PA, Yang J, Metelo AM, Perez-Carro R, Baker R, Wang Z, et al. In vivo HIF-mediated reductive carboxylation is regulated by citrate levels and sensitizes VHL-deficient cells to glutamine deprivation. *Cell Metab* 2013;17:372–85.
38. Le A, Lane AN, Hamaker M, Bose S, Gouw A, Barbi J, et al. Glucose-independent glutamine metabolism via TCA cycling for proliferation and survival in B cells. *Cell Metab* 2012;15:110–21.
39. Metallo CM, Vander Heiden MG. Understanding metabolic regulation and its influence on cell physiology. *Mol Cell* 2013;49:388–98.
40. Metallo CM, Walther JL, Stephanopoulos G. Evaluation of ¹³C isotopic tracers for metabolic flux analysis in mammalian cells. *J Biotechnol* 2009;144:167–74.
41. Young JD, Walther JL, Antoniewicz MR, Yoo H, Stephanopoulos G. An elementary metabolite unit (EMU) based method of isotopically nonstationary flux analysis. *Biotechnol Bioeng* 2008;99:686–99.
42. Fendt SM, Bell EL, Keibler MA, Davidson SM, Wirth GJ, Fiske B, et al. Metformin decreases glucose oxidation and increases the dependency of prostate cancer cells on reductive glutamine metabolism. *Cancer Res* 2013;73:4429–38.
43. McClintock DS, Santore MT, Lee VY, Brunelle J, Budinger GR, Zong WX, et al. Bcl-2 family members and functional electron transport chain regulate oxygen deprivation-induced cell death. *Mol Cell Biol* 2002;22:94–104.
44. Hockel M, Vaupel P. Tumor hypoxia: definitions and current clinical, biologic, and molecular aspects. *J Natl Cancer Inst* 2001;93:266–76.
45. Marin-Valencia I, Yang C, Mashimo T, Cho S, Baek H, Yang XL, et al. Analysis of tumor metabolism reveals mitochondrial glucose oxidation in genetically diverse human glioblastomas in the mouse brain in vivo. *Cell Metab* 2012;15:827–37.
46. Popovici-Muller J, Saunders JO, Salituro FG, Travins JM, Yan SQ, Zhao F, et al. Discovery of the first potent inhibitors of mutant IDH1 that lower tumor 2-HG in vivo. *ACS Med Chem Lett* 2012;3:850–5.
47. Lai K, Selinger DW, Solomon JM, Wu H, Schmitt E, Serluca FC, et al. Integrated compound profiling screens identify the mitochondrial electron transport chain as the molecular target of the natural products manassantin, sesquicillin, and arctigenin. *ACS Chem Biol* 2013;8:257–67.
48. Medes G, Thomas A, Weinhouse S. Metabolism of neoplastic tissue. IV. A study of lipid synthesis in neoplastic tissue slices in vitro. *Cancer Res* 1953;13:27–9.
49. Hatzivassiliou G, Zhao F, Bauer DE, Andreadis C, Shaw AN, Dhanak D, et al. ATP citrate lyase inhibition can suppress tumor cell growth. *Cancer Cell* 2005;8:311–21.
50. Kaelin WG Jr, McKnight SL. Influence of metabolism on epigenetics and disease. *Cell* 2013;153:56–69.
51. Grassian AR, Metallo CM, Coloff JL, Stephanopoulos G, Brugge JS. Erk regulation of pyruvate dehydrogenase flux through PDK4 modulates cell proliferation. *Genes Dev* 2011;25:1716–33.